In situ LA-ICPMS U-Pb dating of sulfates: Applicability of carbonate reference materials as matrix-matched standards

Aratz Beranoaguirre[1,2,3,4], Iuliana Vasiliev[5], Axel Gerdes[2,3]

[1] Institut für Angewandte Geowissenschaften, Karlsruher Institut für Technologie, Adenauerring 20 b, 76131 Karlsruhe, Germany
[2] Institut für Geowissenschaften, Goethe-Universität Frankfurt, Altenhöferallee 1, 60438 Frankfurt am Main, Germany
[3] Frankfurt Isotope and Element Research Center (FIERCE), Goethe-Universität Frankfurt, Frankfurt am Main, Germany
[4] Geologia Saila, Euskal Herriko Unibertsitatea UPV/EHU, Sarriena z/g, 48940 Leioa, Spain
[5] Senckenberg Biodiversity and Climate Research Centre (BiK-F), Senckenberganlage 25, 60325 Frankfurt am Main, Germany

Correspondence to: Aratz Beranoaguirre (aratz.beranoaguirre@kit.edu)

Abstract. Recent developments in analytical capabilities in the field of in situ laser ablation mass spectrometry (LA-ICPMS) have expanded the applications of U-Pb geochronometers in low-U minerals such as carbonates or garnets. The rapid evolution of the technique relies on well-characterized matrix-matched reference materials. In this article, we explore the suitability of using carbonate as "almost-matrix-matched reference materials" for in situ U-Pb dating of sulfates. For such purpose, we have used the astrochronologically dated gypsum and anhydrite samples deposited during the Messinian Salinity Crisis (5.97 – 5.33 Ma) and compared these dates with the U-Pb ages obtained by LA-ICPMS. Although the majority of the samples failed due to the elevated common Pb content and low $^{238}U/^{204}Pb$ ratios, five of the samples showed a higher dispersion on U/Pb ratios. The obtained dates in four of these samples are comparable with the expected ages while another gave an unexpected younger age, each of them with 6-11% of uncertainty. The pit depth of the spots showed that the sulfates ablate similar to carbonates, so the offset due to the crater geometry mismatch or downhole fractionation can be assumed to be negligible. To sum up, the bias between the U-Pb and expected cyclostratigraphic ages, if any, is included in the uncertainty and thus, the results obtained here suggest that carbonate reference material is currently the best option for standardisation of in situ U-Pb sulfate analyses.

1 Introduction

Recent developments in instrumentation and analytical capabilities of LA-ICPMS techniques have greatly expanded the applicability of the U-Pb geochronometer. The high spatial resolution, low cost of analysis and high throughput with relatively good precision (Schaltegger et al., 2015) achievable with the new generation of laser and mass spectrometers favour the study of minerals with low and heterogeneous U concentrations like carbonates or garnets (e.g. Roberts et al., 2020). In fact, carbonate geochronology has gone from scarce publications that involve tedious and long-lasting isotope dilution techniques (e.g., Brannon et al., 1996; Grandia et al., 2000; Woodhead et al. 2006, 2012; Rasbury and Cole, 2009) to a bloom of dozens of publications per year (extensive review in Roberts et al., 2020). Likewise, garnet U-Pb dating is rapidly developing in skarn or metamorphic garnets, with U contents even below 100 parts per billion (e.g., Burisch et al., 2019; Yan et al., 2020; Millonig

et al., 2020). In addition, several laboratories have started to investigate the possibility of measuring other types of minerals: dolomites (Burisch et al., 2017), fluorite (Piccione et al., 2019; Lenoir et al., 2021), nacrite (Piccione et al., 2019) or anatase (Sindern et al., 2019), among others.

The rapid evolution of U-Pb dating in low-U phases is closely related to the availability of reference materials (WC-1 carbonate, Roberts et al., 2017; or Mali garnet, Seaman et al., 2017). Well-characterized matrix-matched reference material is essential for U-Pb analyses by ion probe or laser ablation as sample matrix affects the ablation, transport and ionisation (Sylvester, 2008; Yang et al., 2018). Indeed, LA-ICPMS dates could only be as good as the homogeneity of the reference materials, and the accuracy and precision to which such material is known (Schaltegger et al., 2015). Several authors, however, have appraised the suitability of using non-matrix-matched standardisation, with different levels of success. Deng et al. (2017) and Wafforn et al. (2018) used 91500 and GJ1 zircon, respectively, to correct U/Pb fractionation of garnet and assumed they obtained the correct ages, whereas Yang et al. (2018) measured 11 % too old garnet ages using zircon standardisation. Similarly, Parrish et al. (2018) measured Mud Tank zircon within carbonate analyses and reported a bias between zircon and calcite of c. 4.7%. Piccione et al. (2019) used the WC-1 carbonate reference material for fluorite analysis assuming that the bias between calcite and fluorite may likely be less than the one between calcite and zircon.

This study aims to continue opening new possibilities in the field of in-situ U-Pb dating of low-U minerals, by (I) demonstrating that sulfates can be dated by U-Pb and (II) examining the suitability and reliability of using calcite as "almost matrix-matched reference material" for sulfates. Accurate U-Pb dating of sulfates could contribute to a better understanding of their formation and/or transformation (hydration-dehydration) with the potential of dating diagenetic, pedogenic or tectonic processes. Gypsum ($CaSO_4 \cdot 2H_2O$) and Anhydrite ($CaSO_4$) are the two most abundant sulfates of marine and non-marine evaporite deposits (e.g. Murray, 1963; Babel and Schreiber, 2014). Sedimentary gypsum forms by direct precipitation out of water evaporation under arid climatic conditions in hydrologically restricted environments. Under terrestrial evaporitic conditions, gypsum is the dominant primary mineral and anhydrite forms through gypsum dehydration caused during diagenesis. In the presence of water at shallower levels, the anhydrite is rapidly converted back to gypsum (e.g. Conley and Bundy, 1958; Murray, 1964; Ossorio et al., 2014; Warren, 2016). Although less frequent, non-evaporitic gypsum formation can also take place (see Van Driessche et al., 2019 and references therein).

In the absence of sulfate matrix-matched reference material, we have assumed that the bias between calcite and sulfate is smaller than with the other available reference materials. Both minerals behave very similarly during ablation (e.g., drill speed, U/Pb downhole fractionation, etc.) and ionization in the plasma (Ca^{2+} as the main cation). For evaluating the suitability of the calcite-based corrections, we have analysed gypsum and anhydrite samples from the Messinian Salinity Crisis (MSC) in the Mediterranean Sea (Roveri et al., 2014a, 2014b; Vasiliev et al., 2017; Grothe et al., 2020; Andreetto et al., 2021) and compared them with their astrochronological data (calibrated with astronomically tuned timescales, such as Milankovic cycles, Laskar et al. 1999). Chronostratigraphy of Late Miocene to Early Pliocene within the MSC is well constrained (CIESM, 2008; Manzi et al., 2013, Roveri et al., 2014a) and thus, makes those samples ideal for comparison purposes.

2 Geological Background

The Messinian Salinity Crisis (MSC, 5.97-5.33 Ma) successions record extreme fluctuations in the Mediterranean's paleoceanographic and environmental conditions (e.g. Hsü et al., 1973; Krijgsman et al., 1999; Manzi et al., 2013). At the end of the Miocene, the Mediterranean's connections with the Atlantic Ocean were extremely reduced (e.g. Flecker et al., 2015; Krijgsman et al., 2018) whereas the freshwater supply from the Eastern Paratethys increased (Flecker and Ellam, 2006; Krijgsman et al., 2010). Those paleoceanographic changes lead to the formation of hypersaline water bodies and the deposition of a kilometre-thick evaporite unit (Fig. 1A) (Ryan, 2009). The original definition of the MSC referred to a marked environmental change at the base of the Tripoli diatomite formation (Sicily, Italy) close to the Tortonian/Messinian boundary (Selli, 1960). Astronomical tuning of the pre-evaporitic succession showed that the MSC onset was synchronous throughout the Mediterranean (e.g., Krijgsman et al., 1999; Manzi et al., 2018; Meilijson et al., 2018). According to the shallow water-deep basin model (Hsü et al., 1973; Roveri et al., 2014a), evaporite precipitation was associated with a sea-level drop in the range of 1500 m, up to the almost complete desiccation of the Mediterranean, culminating in halite precipitation and marked by the incisions of deep canyons at the Mediterranean margins. However, a non-evaporitic gypsum formation during MSC has been also described (Hsü et al., 1973). Isotope analyses of gypsum hydration water and the salinity of fluid inclusions in MSC gypsum indicate large freshwater inputs during gypsum formation (Natalicchio et al., 2014; Evans et al., 2015; Costanzo et al., 2019). Additionally, suggestions of the important role of sulfur-oxidizing bacteria in biogeochemically meditated gypsum formation (Grothe et al., 2020) are increasingly used to explain a low salinity, yet high concentrations of Ca^{2+} and SO_2^{4-} (Clauer et al., 2000), during the formation of MSC evaporites.

According to previous publications (Roveri et al., 2008a, 2008b and 2014a), the MSC can be separated into three main stages (Fig. 1B). Stage I (5.97-5.60Ma), the so-called Primary Lower Gypsum (PLG, Lugli et al., 2010), is defined by the deposition of primary selenite gypsum unit. During the stage II (5.60-5.55 Ma), large evaporite deposits occurred (Resedimented Lower Gypsum unit, RLG), which includes halite, gypsum cumulates and brecciated limestones ('Calcare di Base' type 3, Manzi et al., 2011). Likewise, clastic gypsum derived from the dismantlement of the PLG unit can be found within this stage. Finally, alternating gypsum (mainly bottom grown selenite and cumulate) and fine- to coarse-grained terrigenous deposits form the Upper Gypsum unit (UG, stage III, 5.55-5.33 Ma). There is no outcrop with the complete section of the MSC, but different segments are well exposed throughout the Mediterranean

3 Methodology

U-Pb data was acquired in situ in polished mounts and slabs using a RESOLution 193 nm ArF excimer laser (CompexPro 102) equipped with a two-volume ablation cell (Laurin Technic S155) coupled to a (I) single collector (SC)-ICPMS (ElementXR, ThermoScientific) or (II) multicollector (MC)-ICPMS (Neptune Plus, ThermoScientific) at FIERCE (Frankfurt Isotope & Element Research Center), Goethe University Frankfurt. The method is modified after Ring and Gerdes (2016) and Burisch et al. (2017). Samples are pre-screened in order to identify sub-zones with a higher $^{238}U/^{206}Pb$ ratio before each analytical session.

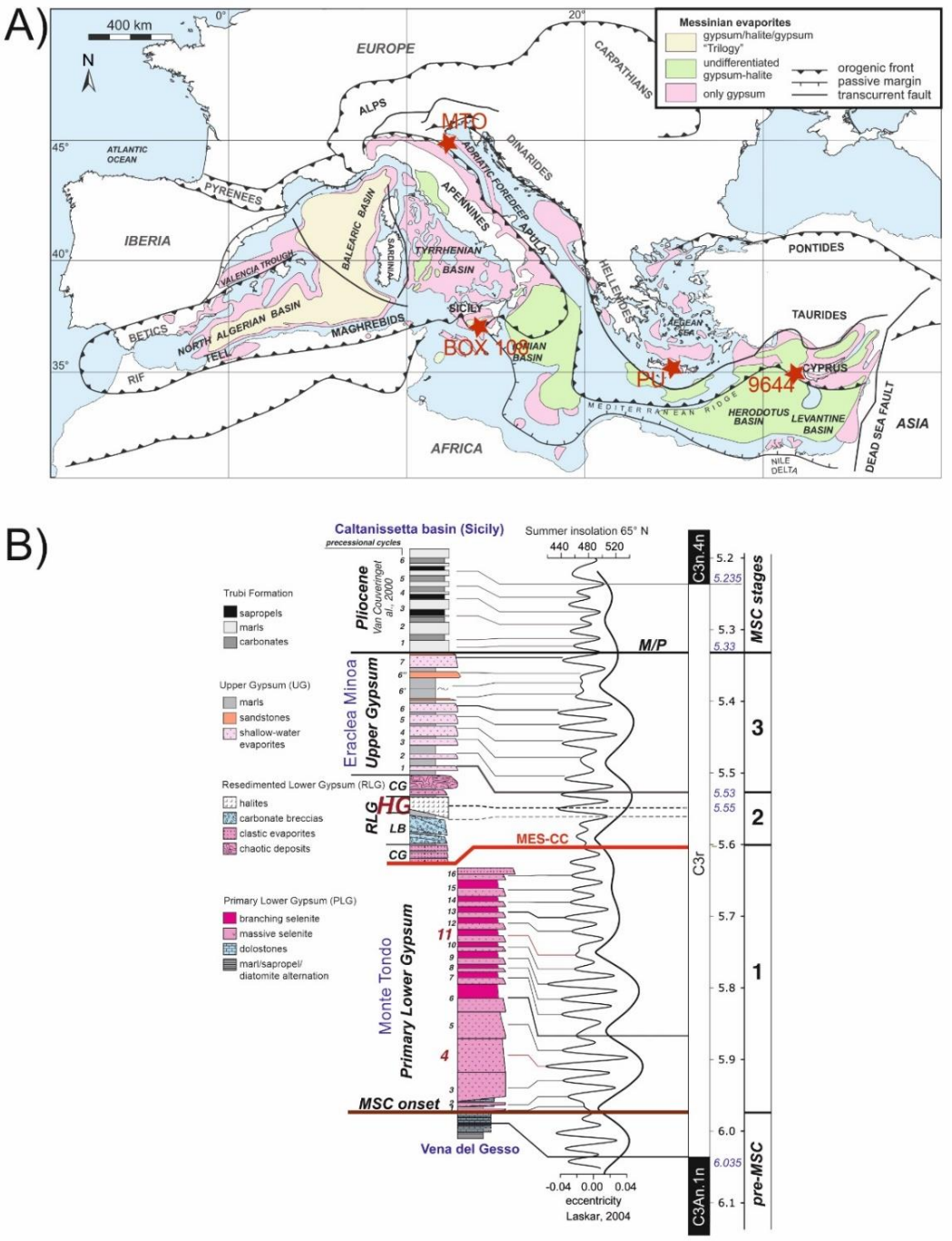

Fig. 1: A) Geological sketch of the Messinian evaporite deposits along the Mediterranean Sea (modified after Rouchy and Caruso, 2006). Note that only the successfully dated sample locations are shown. B) Chronostratigraphy of Late Miocene to Early Pliocene with MSC events in the Mediterranean (modified from Vasiliev et al., 2017).

The first sessions, between December 2019 and May 2020, were performed with the SC-ICPMS. Prior to the measurements, signal strength was tuned for maximum sensitivity while keeping oxide formation below ~ 0.5 % (UO/U) and element fraction low (e.g. Th/U ~ 0.9). This was done by ablating at 3 µm/s with a 60 µm spot at 6 Hz and 3.5 J/cm^2 fluence in the glass SRMNIST 612 (Jochum et al., 2011). The average sensitivity obtained for the line is ca. 100,000 cps per µg/g for ^{238}U. The detection limits (4 x background signal) of the instrument for ^{206}Pb and ^{238}U were c. 0.3 and 0.03 ng/g. Data were acquired in fully-automated mode overnight. Each analysis consists of 18 s background acquisition followed by 18 s of sample ablation and 20 s washout. During 36 s data acquisition, the signal of ^{206}Pb, ^{207}Pb, ^{208}Pb, ^{232}Th and ^{238}U were detected by peak jumping in simultaneous analogue and pulse counting mode. Detailed data acquisition parameters are summarised in Table 1.

Due to the low precision obtained in those sessions, where only two samples from a single session can be considered acceptable (see results and discussion), the use of the more sensitive MC-ICPMS (Craig et al., 2018, 2020) was deemed necessary for subsequent measurements. The sessions with the MC-ICPMS were carried out between July 2020 and December 2020. As for the single collector, signal strength was tuned for maximum sensitivity while keeping oxide formation below ~ 0.5 % (UO/U) and element fraction low (e.g. Th/U ~ 0.9). In that case, it was done with a 35 µm, 6 Hz, ca. 3.5 J/cm^2 fluence and a 3 µm/s line ablated in the glass SRMNIST 614 (Jochum et al., 2011). The average sensitivity obtained for the line is ca. 120,000 cps per µg/g for ^{238}U (note the smaller spot size compare to the SC-ICPMS). The detection limits in the multicollector ICPMS were c. 0.3 and 0.01 ng/g for ^{206}Pb and ^{238}U, respectively. The analyses were done during 31 s (15 s background and 16 s of ablation) in static mode, measuring ^{206}Pb and ^{207}Pb with Secondary Electron Multipliers (SEMs), ^{202}Hg and ^{204}Pb with Multiple Ion Counters (MICs) and ^{232}Th and ^{238}U on Faraday cups with 10^{13} Ω amplifiers. Faraday signals in V are converted into cps by using a factor of 62,400,000. Detailed data acquisition parameters are summarised in Table 2.

In each analytical session, soda-lime glass SRMNIST614 was used as the primary reference material to correct for mass bias (^{207}Pb/^{206}Pb) and the interelement fractionation and instrumental drift (^{206}Pb/^{238}U) throughout the entire analytical session. Carbonate reference material WC-1 (254 Ma, Roberts et al., 2017) was used to determine the difference of the Pb/U fractionation between carbonate and synthetic glass matrix. Depending on the analytical conditions (i.e, spot size, laser fluence, torch position, sample gas flows, etc.) the matrix effect can vary up to 12 % (FIERCE laboratory observation, e.g. Cruset et al. 2021) and even at similar tuning parameters, two sessions separated by some weeks could result in different Pb/U correction factors. So far, this behaviour is not very well understood and due to its unpredictability, the matrix correction is calculated for each session (see below). Secondary reference calcite materials, ASH-15D calcite (2.965 ± 0.011 Ma, Nuriel et al., 2021), B-6 (42.99 ± 0.99 Ma, only LA-ICPMS data, Pagel et al., 2018) and in-house calcite (reproducible age of ca. 36 Ma) were measured for quality control. Not all the secondary reference materials were used in each session (see information in Tables 1 and 2).

Laboratory & Sample Preparation	
Laboratory name	FIERCE, Frankfurt Isotope & Element Research Center Goethe Univesität, Frankfurt am Main
Sample type/mineral	Sulphate
Sample preparation	25 mm polished resin mounts
Imaging	Petrographic microscope & 2400 dpi digital scan
Laser ablation system	
Make, Model & type	RESOlution ArF excimer laser (COMpex Pro 102)
Ablation cell	Two-volume ablation cell (Laurin Technic S155)
Laser wavelength	193 nm
Pulse width	20 ns
Fluence	2 J/cm^2
Repetition rate	10 Hz
Pre-ablation	4 pulses (same parameters as main ablation)
Ablation duration	18 s
Ablation rate	~ 0.6 µm/s (in the primary RM), ~ 0.9 µm/s (in carbonate and sulfate)
Spot shape & size	Round, 154 µm (diameter)
Sampling mode	Static spot ablation
Gasses	Sample cell: He. Funnel: He + Ar. Tubbing: He + Ar + N_2
Gas flows	He (300 ml/min), Ar (1050 ml/min), N_2 (8 ml/min).
ICP-MS Instrument	
Make, Model & type	ThermoScientific ElementXr sector field ICP-MS
Sample introduction	Ablation aerosol
RF power	1300 W
Detection system	Secondary electron multiplier (with conversion dynode at -8kV). Simultaneous analogue and counting (pulse) modes of detection (conversion factors calculated per mass and applied offline). Magnetic field fixed. Detection by peak jumping with electrostatic analyzer.
Masses measured	206, 207, 232, 238
Dwell times	206: 6.4 ms, 207: 7.5 ms, 232: 2.0 ms, 238: 4.6 ms
Samples per peak/integration type	4 for all masses/average
Total time per run	99 ms
Number of runs/total time	370 / 36.6 s
Acquisition mode	Trigger from laser (20 s after pre-ablation), background: 18 s, ablation: 18 s
Dead time	29 ns
Data Processing	
Gas blank	20 s on-peak zero subtracted.
Calibration strategy	SRMNIST614 as primary RM, WC-1 as offset RM, and ASH15D as validation RM.
Reference Material (RM) information	Soda-lime glass SRMNIST614 (Jochum et al., 2011), WC-1 (Roberts et al., 2017), ASH15D (Nuriel et al., 2021)
Data processing / LIEF correction	In-house VBA spreadsheet program (Gerdes and Zeh, 2006, 2009). Intercept method for LIEF correction, assumes Pbc corrected WC-1 and samples behave identically.
Mass discrimination	$^{207}Pb/^{206}Pb$ (0.2%) and $^{206}Pb/^{238}U$ (5%) normalised to primary standard
Common-Pb correction	No common-Pb correction applied to the data.
Uncertainty level & propagation	Uncertainties are quoted at 2σ absolute and are propagated by quadratic addition of the within run precision (SD of the mean of ratios in log-ratio space), counting statistics, background, common Pb correction (if applicable) and the excess of scatter (calculated from the primary RM). In addition, an excess of variance of 1.45 % (1σ), calculated from the offset RM, was added quadratically to the $^{206}Pb/^{238}U$ ratios. Systematic uncertainties are reported as an expanded uncertainty, considering long term reproducibility (1.5%, 2σ) and decay constant uncertainties.
Quality control / Validation	WC-1: 254.7 ± 2.3 / 4.4 Ma (2s, MSWD = 1.00, n = 28) ASH15D: 3.004 ± 0.153 / 0.159 Ma (2s, MSWD = 0.85, n = 28) (Ages are the $^{206}Pb/^{238}U$ lower intercept ages of the calculated isochrons with the concordia curve in the Tera-Wasserburg space)

Table 1: LA-SC-ICPMS U-Pb analysis procedure at Goethe University Frankfurt, FIERCE laboratory.

Laboratory & Sample Preparation	
Laboratory name	FIERCE, Frankfurt Isotope & Element Research Center Goethe Univesität, Frankfurt am Main
Sample type/mineral	Sulphate
Sample preparation	25 mm polished resin mounts and polished thick sections
Imaging	Petrographic microscope & 2400 dpi digital scan
Laser ablation system	
Make, Model & type	RESOlution ArF excimer laser (COMpex Pro 102)
Ablation cell	Two-volume ablation cell (Laurin Technic S155)
Laser wavelength	193 nm
Pulse width	20 ns
Fluence	2 J/cm^2
Repetition rate	10 Hz
Pre-ablation	2 pulses (same parameters as main ablation)
Ablation duration	16 s
Ablation rate	~ 0.6 µm/s (in the primary RM) ~ 0.9 µm/s (in carbonate and sulfate)
Spot shape & size	Round, 130 µm (75 µm for primary RM), except for session 1 (90 µm for all spots)
Sampling mode	Static spot ablation
Gasses	Sample cell: He. Funnel: He + Ar. Tubbing: He + Ar + N_2
Gas flows	He (300 ml/min), Ar (~950 ml/min), N_2 (5-10 ml/min). Ar and N_2 are tunned each session, so the values can be slightly different
ICP-MS Instrument	
Make, Model & type	ThermoScientific Neptune Plus multi-collector ICP-MS
Sample introduction	Ablation aerosol
RF power	1300 W
Detection system	Simultaneous multi-collection. Secondary Electron Multipliers (SEMs) for ^{206}Pb and ^{207}Pb Multiple Ion Counters (MICs) for ^{202}Hg and ^{204}Pb Faraday cups with 10^{13} Ω amplifiers for ^{232}Th and ^{238}U
Masses measured	202, 204, 206, 207, 232, 238
Total time per run	131 ms
Number of runs/total time	230 / 30.1 s
Acquisition mode	Trigger from laser (14 s after pre-ablation), background: 15 s, ablation: 16 s
Data Processing	
Gas blank	15 s on-peak zero subtracted.
Calibration strategy	SRMNIST614 as primary RM, WC-1 as offset RM, and ASH15D, B6 & in-house calcite as validation RM.
Reference Material (RM) information	Soda-lime glass SRMNIST614 (Jochum et al., 2011), WC-1 (Roberts et al., 2017), ASH15D (Nuriel et al., 2021), B-6 (Pagel et al., 2018), CalBraun (in-house calcite RM)
Data processing / LIEF correction	In-house VBA spreadsheet program (Gerdes and Zeh, 2006, 2009). Intercept method for LIEF correction, assumes Pbc corrected WC-1 and samples behave identically.
Mass discrimination	^{207}Pb/^{206}Pb and ^{206}Pb/^{238}U normalised to primary standard (variable in each session)
Common-Pb correction	No common-Pb correction applied to the data.
Uncertainty level & propagation	Uncertainties are quoted at 2σ absolute and are propagated by quadratic addition of the within run precision (SD of the mean of ratios in log-ratio space), counting statistics, background, common Pb correction (if applicable) and the excess of scatter (calculated from the primary RM). In addition, an excess of variance calculated for each session from the offset RM, was added quadratically to the ^{206}Pb/^{238}U ratios. Systematic uncertainties are reported as an expanded uncertainty, considering long term reproducibility (1.5%, 2σ) and decay constant uncertainties.
Quality control / Validation	Session 1: WC-1: 254.8 ± 1.9 / 4.3 Ma (2s, MSWD = 1.0, n = 12) B-6: 42.73 ± 0.59 / 0.87 Ma (2s, MSWD = 0.84, n = 12) CalBraun: 36.72 ± 1.23 / 1.35 Ma (2s, MSWD = 0.89, n = 12) Session 2: WC-1: 254.1 ± 2.0 / 4.4 Ma (2s, MSWD = 1.0, n = 20) B-6: 42.66 ± 0.47 / 0.80 Ma (2s, MSWD = 0.50, n = 22) CalBraun: 36.07 ± 0.65 / 0.85 Ma (2s, MSWD = 0.61, n = 22) Session 3: WC-1: 254.5 ± 3.2 / 5.0 Ma (2s, MSWD = 1.0, n = 10) ASH15D: 3.060 ± 0.193 / 0.198 Ma (2s, MSWD = 1.0, n = 10) B-6: 43.54 ± 0.79 / 1.02 Ma (2s, MSWD = 1.13, n = 10) Session 4: WC-1: 254.5 ± 1.6 / 4.1 Ma (2s, MSWD = 1.0, n = 20) ASH15D: 3.091 ± 0.102 / 0.112 Ma (2s, MSWD = 0.88, n = 20) B-6: 43.83 ± 0.39 / 0.77 Ma (2s, MSWD = 0.56, n = 20) (Ages are the ^{206}Pb/^{238}U lower intercept ages of the calculated isochrons with the concordia curve in the Tera-Wasserburg space. WC-1 RM are anchored at 0.85 value of ^{207}Pb/^{206}Pb)

Table 2: LA-MC-ICP-MS U-Pb analysis procedure at Goethe University Frankfurt, FIERCE laboratory.

Raw data were corrected offline using an in-house VBA spreadsheet program (Gerdes and Zeh, 2006, 2009). Following background and interferences corrections, outliers (±2σ) were rejected based on the time-resolved $^{207}Pb/^{206}Pb$ and $^{206}Pb/^{238}U$ ratios and the Pb and U signal. All in all, five sessions were performed, and the matrix Pb/U correction factors (carbonate vs SRMNIST glass) applied to each of them are as follows: 4.5 % for SC-ICPMS session, 8 % for MC-ICPMS session 1 (same spot size for both carbonate and SRMNIST glass, see Table 2), 0.5 % for session 2 (different spot size, Table 2), 0 % for session 3, and 0 % for session 4. The $^{206}Pb/^{238}U$ downhole fractionation during 16/18 s depth profiling was estimated to be 3%, based on the common Pb-corrected WC-1 analyses, and was applied as an external correction to all sulfates analyses and secondary reference materials. Uncertainties for each isotopic ratio are the quadratic addition of the within-run precision, counting statistic uncertainties of each isotope, and the excess of scatter and variance (Horstwood et al., 2016) calculated from the SRMNIST 614 and the WC-1 after drift correction. To account for the long-term reproducibility of the method we added by quadratic addition an expanded uncertainty of 1.5% to the final age of all analysed samples (Montano et al., 2021). This was deducted from repeated analyses of ASH-15D in the FIERCE laboratory between 2017 and 2019. Data were displayed in Tera-Wasserburg plots and ages were calculated as lower concordia-curve intercepts using the same algorithms as Isoplot 4.15 (Ludwig, 2012). All uncertainties are reported at the 2σ level. After the analysis, the depth of the ablation pit was measured in several spots per sample, including the WC-1 and SRMNIST 614 reference materials, using the Keyence VHX 6000 digital microscope.

4 Samples and results

4.1 U-Pb Dating

U-Pb dating was applied to 32 samples from the different locations and all available gypsum/anhydrite varieties (large selenite crystals, banded selenite, gypsum cumulates, anhydrite, halite with gypsum and anhydrite intercalation) across the Mediterranean Sea (Fig. 1), which display variable contents of Pb and U. Only five of them were successfully dated (15 % of success). The undatable samples are characterized by analyses that clustered near the common Pb intercept, disclosing a large amount of common Pb (Fig. 2). This low μ ($^{238}U/^{204}Pb$ ratio) makes it impossible to draw any regression line. No link between successful/unsuccessful samples and their texture could have been established and both successful and unsuccessful samples have been found within the same type of gypsum. The successfully dated samples are described below, and their results are presented in Fig. 3 as well as in supplementary Tables S1 and S2.

4.1.1 Sample MTO 4-4

The MTO 4-4 sample was collected at the Monte Tondo gypsum quarry, located within the Vena del Gesso basin (along the western Romagna Apennines), and belongs to the PLG (Lugli et al., 2007, 2010; Vasiliev et al., 2017). It is a banded selenite (type F4 of Lugli et al., 2010) and the cyclostratigraphic age is 5.92 Ma, close to the onset of the MSC. The sample was measured in three different sessions. The maximum U and Pb content on the analysed spots are 2.34 μg/g and 3.85 μg/g,

respectively, depicting a maximum U/Pb ratio of 98.4 in the best case. The first of the sessions was measured with the SC-ICPMS and the analyses define a regression line with a lower intercept at 6.01 ± 1.19 Ma (±2σ, MSWD = 1.07, Fig. 3). The other two sessions were measured with the MC-ICPMS and the lower intercept of the regression lines are 5.55 ± 0.61 Ma (±2σ, MSWD = 1.00, Fig. 3) and 5.73 ± 0.37 Ma (±2σ, MSWD = 1.13, Fig. 3).

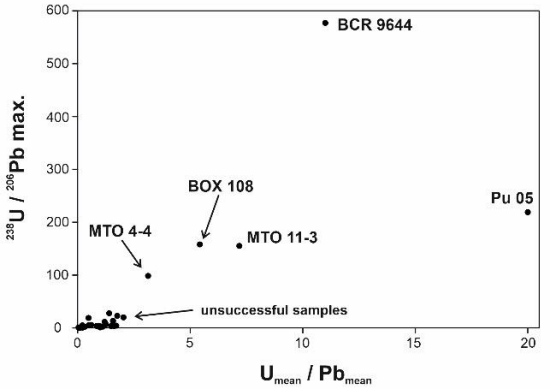

Fig. 2: Diagram showing $U_{mean\ content}/Pb_{mean\ content}$ vs. maximum value on $^{238}U/^{206}Pb$ axis. The successfully dated samples have a distinctively higher U/Pb heterogeneity.

4.1.2 Sample MTO 11-3

This sample was also collected by Vasiliev et al., (2017) at the Monte Tondo gypsum quarry. It is a massive selenite (F3 of Lugli et al., 2010) and belongs to the younger cycles of the PLG. Its estimated cyclostratigraphic age is 5.701 Ma. MTO 11-3 was measured as well in three different sessions. The maximum U and Pb content on the analysed spots are 5.49 µg/g and 0.97 µg/g, respectively, depicting a maximum U/Pb ratio value of 155.2 in the best case. The first of the sessions was measured with the SC-ICPMS and the analyses define a regression line with a lower intercept at 5.40 ± 0.84 Ma (±2σ, MSWD = 1.13, Fig. 3). The other two sessions were measured with the MC-ICPMS and the lower intercept of the regression lines are 5.46 ± 0.44 Ma (±2σ, MSWD = 1.41, Fig. 3) and 5.55 ± 0.32 Ma (±2σ, MSWD = 1.03, Fig. 3).

4.1.3 Sample BOX 108

BOX 108 is a halite with anhydrite nodules. It comes from the borehole EMS-4 (Cattolica Eraclea) in the Caltanissetta Basin (southwest of Sicily) and was donated to Prof. Cita (University of Milano). The core was drilled from - 82 m to -665 m below sea level and the sample was located almost at the bottom (approximately at - 610 m). Cyclostratigraphic ages point to 5.55-5.60 Ma. The analyses were made both in halite and in anhydrite, but only the anhydrite was successful. It was measured twice with the MC-ICPMS. The maximum U and Pb content on the analysed spots are 5.70 µg/g and 1.67 µg/g, respectively, depicting a maximum U/Pb ratio value of 158.0 in the best case. The analyses define a regression line with a lower intercept at 5.55 ± 0.35 Ma (±2σ, MSWD = 1.01, Fig. 3) in the first of the sessions and 5.54 ± 0.38 Ma (±2σ, MSWD = 1.49, Fig. 3) in the second.

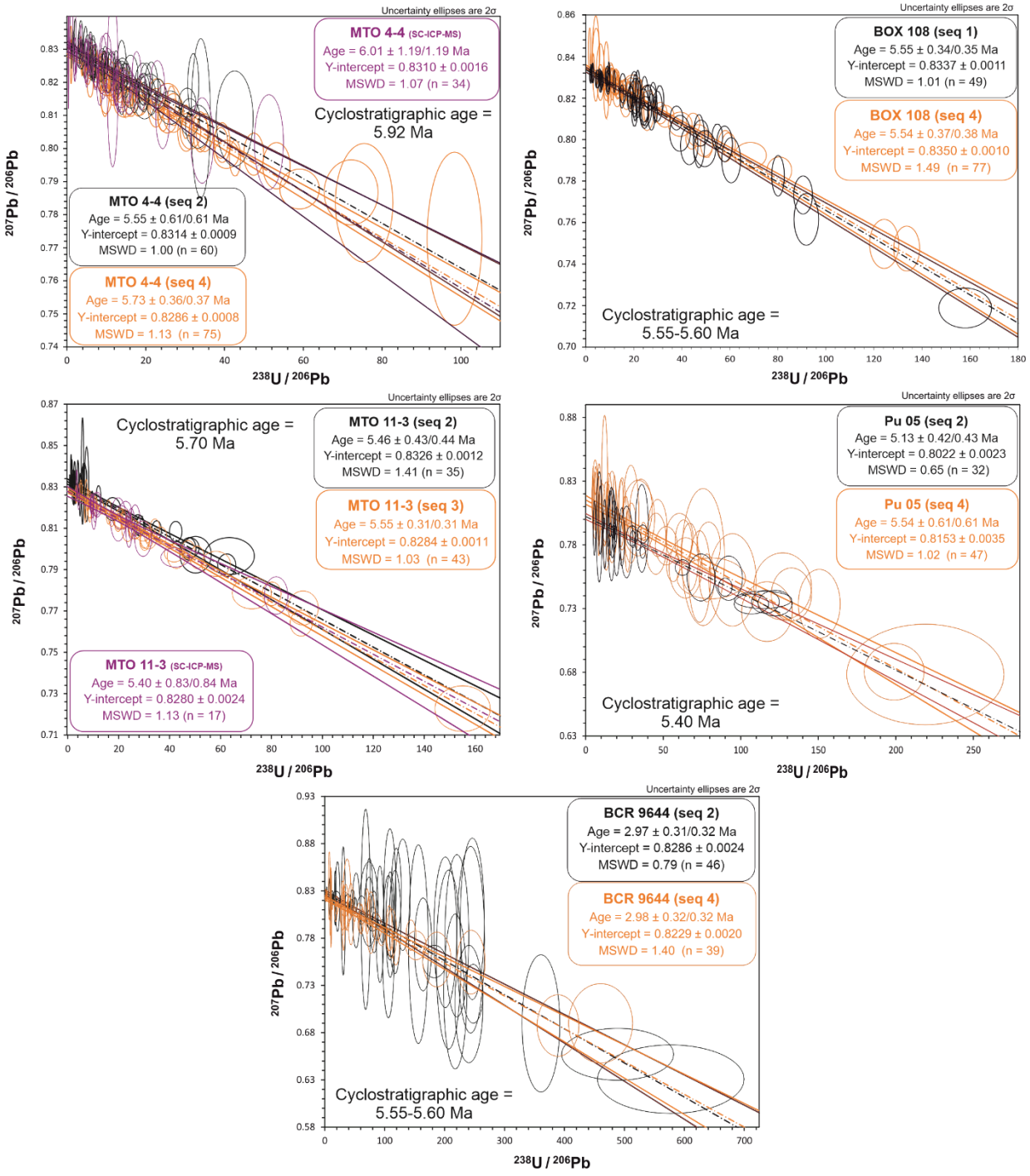

Fig. 3: Tera-Wasserburg diagram ($^{207}Pb/^{206}Pb$ vs. $^{238}U/^{206}Pb$) for the samples MTO 4-4, MTO 11-3, BOX 108, Pu 05 and BCR 9644. The blue ellipses and error envelope in samples MTO 4-4 and MTO 11-3 correspond to the analyses with the SC-ICPMS, while the orange and black colours refer to two independent sessions with the MC-ICPMS. Both propagated within-session uncertainties and the expanded uncertainties are ±2σ .

4.1.4 Sample BCR9644

The sample BCR9644 was collected from the cores of Deep Sea Drilling Program Site 42A hole 376 cored in 1975 West of Cyprus and stored at Bremen International Ocean Drilling Program repository. BCR9644 was collected from a Gypsum Breccia, at 170.28 m below sea level and has a stratigraphic age of ca. 5.55 - 5.60 Ma. It was measured twice with the MC-ICPMS. The maximum U and Pb content on the analysed spots are 2.31 µg/g and 0.61 µg/g, respectively, although Pb rarely exceeds 0.1 µg/g. The maximum U/Pb ratio obtained in that sample is 577.5 in the best case. The low Pb contents imply large error ellipses, but successful regression lines have been defined, with a lower intercept at 2.98 ± 0.34 Ma (±2σ, MSWD = 0.79, Fig. 3) in the first of the sessions and 2.98 ± 0.32 Ma (±2σ, MSWD = 1.40, Fig. 3) in the second.

4.1.5 Sample Pu 05

This sample was collected in the Ploutis region (Central Crete, Greece) and it is a gypsum breccia. The stratigraphic age of these gypsum units is disputed between being part of the PLG (Zachariasse et al., 2008) but the texture is direct capping by Lago Mare deposits strongly suggest that Pu 05 belongs to the UG unit. Its Cyclostratigraphic age is ca. 5.40 Ma. Pu 05 was also measured twice with the MC-ICPMS. The maximum U and Pb content on the analysed spots are 1.44 µg/g and 0.16 µg/g, respectively, depicting a maximum U/Pb ratio value of 158.0 in the best case. Each session defines a regression line with a lower intercept at 5.15 ± 0.42 Ma (±2σ, MSWD = 0.68, Fig. 4) and 5.54 ± 0.61 Ma (±2σ, MSWD = 1.02, Fig. 4), respectively.

4.2 Pit depth measurements

After the analyses, pit depths were measured in all the samples as well as in the carbonate reference materials. The measured pit depth averages were used for calculating the U and Pb contents (Tables 3 and 4). The shape and depth of the craters in WC-1 primary carbonate are all similar and their average depth is 15.0 µm (SD = 1.34, n = 16). Few spots corresponding to the secondary reference materials were also checked and they are comparable to those of WC-1. The pits of the SRMNIST 614 are ca. 33% shallower than the ones in the calcite matrix, around 10 µm deep. Regarding the sulfate samples, the pit depth of samples MTO 4-4 and MTO 11-3 is rather homogeneous with mean values of 29.6 µm (SD = 6.2, n = 44) and 18.9 µm (SD = 5.9, n = 37, Fig. 4A), respectively. The samples BCR 9644 and BOX 108 display zones with different heights in some of the ablation holes (Fig. 4B). Although they are exceptional, two ca. 90 µm and two ca. 60 µm pits were measured in BOX 108. Considering them, the average depth is 28.2 µm (SD = 16.4, n= 64) whereas excluding those four heights the standard deviation improves substantially (25.0 µm, SD = 8.8, n = 60). The average depth for the sample BCR 9644 is 16.2 µm (SD = 6.7, n=32) excluding two ca. 60 µm spots. On the other hand, the sample PU 05 shows higher variability and larger standard deviation, since the pit depth varies from 29 µm to 107 µm. The calculated average is 62.6 µm (SD = 23.0, n = 48).

5 Discussion

5.1. Low success rate

5.1.1. High common Pb content and potential applicability

The majority of the analysed samples, 27 out of 32, were unsuccessful due to the high common Pb content and hence, low or non-existent spread in the $^{238}U/^{206}Pb$ axis. Recent studies in the field of environmental hazards have shown that Pb tends to incorporate into sulfates, both gypsum and anhydrite (Astilleros et al., 2010; Morales et al., 2014; Kameda et al., 2017). In fact, in presence of high-Pb fluids, anglesite ($PbSO_4$) is simultaneously intergrown with those sulfates. The behaviour of U remains unknown, although experiments carried out on phosphogypsum, a waste by-product generated from apatite in the production process of phosphoric acid and phosphate fertilizers, suggest that U uptake by gypsum is pH controlled (Lin et al., 2018). Thus, the more alkaline the environment is the higher U concentration could be expected in gypsum. However, the pH of evaporating seawater rarely reaches those values and tends to drop as the evaporation process goes on (Babel and Schreiber, 2014). Considering a low salinity, but high concentrations of Ca^{2+} and SO_2^{4-} (Clauer et al., 2000) during the formation of MSC evaporites, the alkalinity of the depositional environment might have increased. In any case, even the gypsum precipitated in U-rich environments like uranium mine tailings contain a high amount of Pb among other metals (Liu and Hendry, 2011).

The amount of common Pb is a challenge for dating young rocks, as their success strongly depends on the spread in the X-axis ($^{238}U/^{206}Pb$). In turn, given the same initial $^{238}U/^{206}Pb$ ratio, older samples would have produced sufficient radiogenic Pb, and thus, a certain spread in the Y-axis ($^{207}Pb/^{206}Pb$) as to be projected in a more precise regression line. Indeed, older samples are more influenced by the $^{207}Pb/^{206}Pb$ ratio and therefore, it is highly likely that the success rate increases with the age of the sample.

5.1.2. SC-ICPMS vs. MC-ICPMS

The first set of samples was measured with the SC-ICPMS. The U and Pb contents in the samples were rather low and produce large error ellipses in every single spot. This issue, together with low μ ratios (i.e., spread on $^{238}U/^{206}Pb$), produces substantial uncertainties in the final ages (Fig. 3) and a comparison with the depositional ages is poor. In order to achieve better results, we decided to accomplish subsequent measurements with the MC-ICPMS, which provides about three times better sensitivity and simultaneous isotope detection (Craig et al., 2018; 2020). The higher sensitivity implies smaller uncertainties in each spot and hence, more accurate and precise regression lines (i.e., ages) can be depicted.

Indeed, the improvement in age precision is clearly illustrated in Fig. 3. Although the results can be biased because fewer data were acquired during SC-ICPMS analyses, given a similar spread in the $^{238}U/^{206}Pb$ axis, the uncertainties of c. 15 % (MTO 11-3) or 20 % (MTO 4-4) obtained with the SC-ICPMS were reduced to 8 % (MTO 11-3, seq 2) and 11 % (MTO 4-4, seq 2) by using the MC-ICPMS (Fig. 3). Furthermore, the re-measurement of these two samples in another independent session in which higher $^{238}U/^{206}Pb$ ratios were found, reduced the uncertainties even more down to ca. 6%.

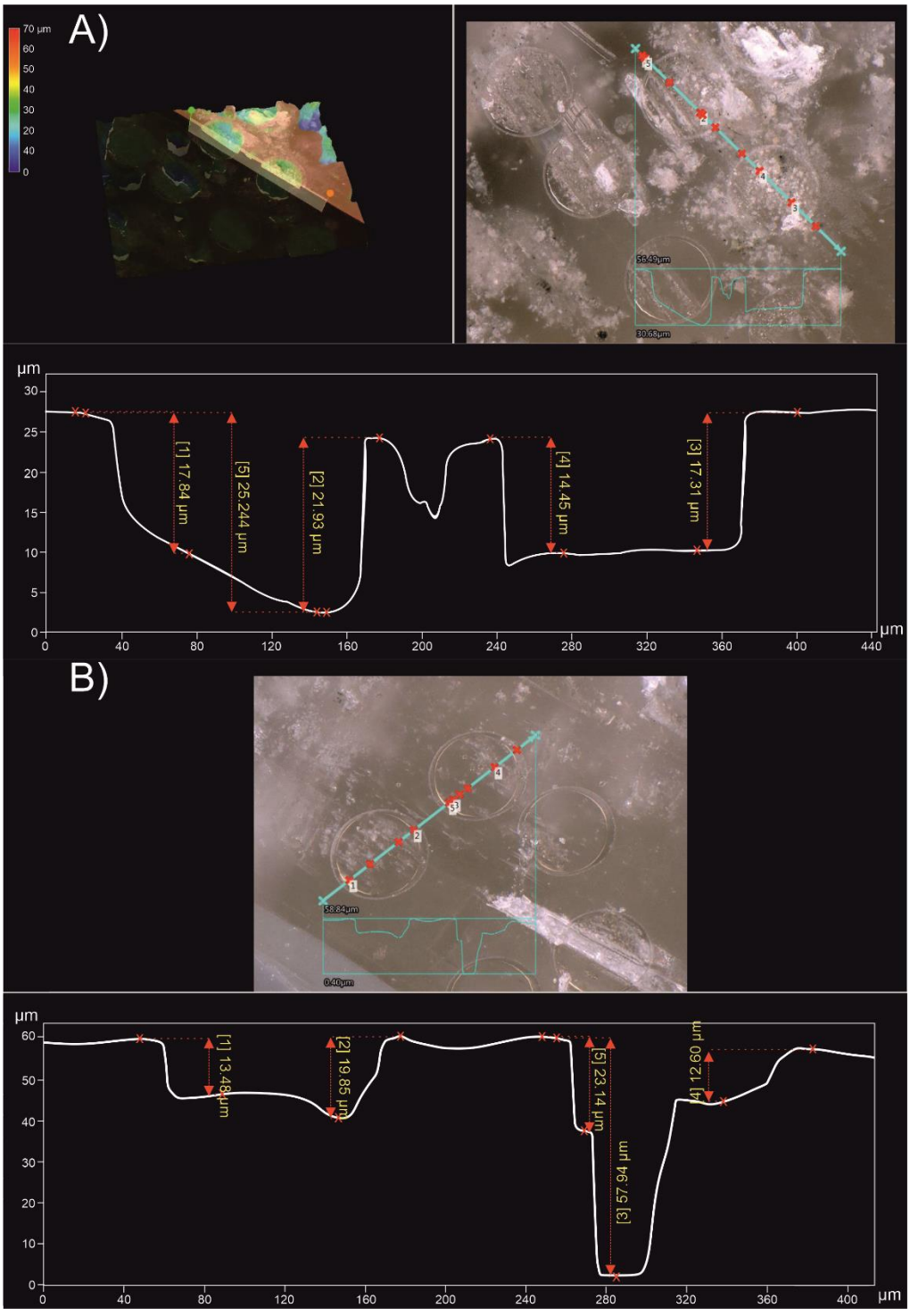

Fig. 4: Pit depth profile of the samples MTO 11-3 (a) and BCR 9644 (b). Whereas the pit shape is roughly homogeneous in the MTO 11-3, the sample BCR 9644 displays deeper areas in some of the pits. The profiles are measured using a Keyence digital microscope VHX-6000.

5.2 U-Pb ages vs cyclostratigraphic ages

Well-characterized matrix-matched reference material is essential for U-Pb analytical techniques using laser probes as matrix differences between sample and reference standard can cause a significant offset in the obtained ages (Yang et al., 2018; Guillong et al., 2020). However, in the absence of sulfate reference materials, an attempt to use calcite reference materials was carried out, expecting that the offset between both materials was going to be low or negligible. The light absorption observed in calcite and gypsum is similar and they are easily ablated even at low fluence (less than 2 J/cm^2). As a comparison, Piccione et al. (2019) obtained analogous ages on contemporary fluorite and nacrite, both corrected to the same calcite reference material, even when the fluorite has different light absorption and higher energy is needed for its ablation (5-6 J/cm^2). Due to those reasons, we expected a significantly lower matrix-induced offset than the one observed between calcite and zircon (4.7 %, Parrish et al., 2018).

The cyclostratigraphic ages of the MSC samples are well-known (e.g. Vasiliev et al. 2017) and we have used them for testing the suitability of the corrections with respect to carbonate matrix. As pointed out above, the majority of the samples contain a significant amount of common Pb and only five ages were obtained. Although the µ-values of those samples were only moderate, the individual uncertainties range between 6 to 11 % and the ages obtained for the samples MTO 4-4, MTO 11-3, Pu 05 and BOX 108 are in accordance with the cyclostratigraphic ages (e.g. Lugli et al., 2007; Vasiliev et al., 2017). A direct comparison of the U-Pb and cyclostratigraphic ages (Fig. 5), however, points to a slight bias toward younger ages, suggesting a systematic offset between both. Taken singly, each U-Pb date overlaps the cyclostratigraphic age, but a more precise measure is the inverse variance weighted mean of all ten discrepancies between the two ages. The calculated weighted average, i.e. the mean discrepancy, is -0.14 ± 0.14 Ma (±2σ, MSWD = 0.77). This can now have both an analytical and a geological significance; it can be interpreted as I) matrix mismatch between carbonate and sulfate or II) dating of a subsequent event instead of sedimentation. In fact, the mobilisation of U and Pb during sediment compaction causes some U/Pb heterogeneity, which improves or enables the possibility of dating these sediments by the U-Pb method. The small mean age discrepancy obtained on the sulfate samples is in line with that reported from Montano et al. (2022) on lacustrine carbonates. In this study, although overlapping within uncertainties, a systematic offset was found between U-Pb ages of carbonate cement and that of zircon from ash layers. Thus, U-Pb ages of carbonate and sulfate cement likely dates early diagenesis and not the sediment deposition. This supports our hypothesis that there is no difference in U-Pb fractionation between sulfate and carbonate matrix, although it is not direct evidence.

On the other hand, the sample BCR 9644 resulted in an unexpected younger age of ca. 3 Ma. The brecciated nature of the sample, together with its extremely low Pb content (0.03 µg/g on average) in comparison with surrounding samples suggest a subsequent (re)crystallization and remobilization of U and Pb that could be related to the breccia formation. Warthman et al. (2000) proposed an important bacterial activity after the evaporite formation. For the equivalent in time Site 374, located South-East Sicily, an ~3 m thick dolomitization front in Pliocene hemipelagic succession overlying the UG was identified. Here, a hypothesized role of the deep biosphere, sulfate-reducing bacteria thriving on the dissolution of sulfate-bearing

minerals (Warthman et al., 2000; Petrash et al., 2017) was suggested. Montano et al. (2019, 2021) showed that biological activity may control the U-Pb partitioning on carbonates, so the connection between the bacterial activity and the 3 Ma age could not be discarded. Although gypsum to anhydrite to gypsum (two-step) transformation can be considered as another possible scenario, there is no observation neither in the literature, that supports this hypothesis.

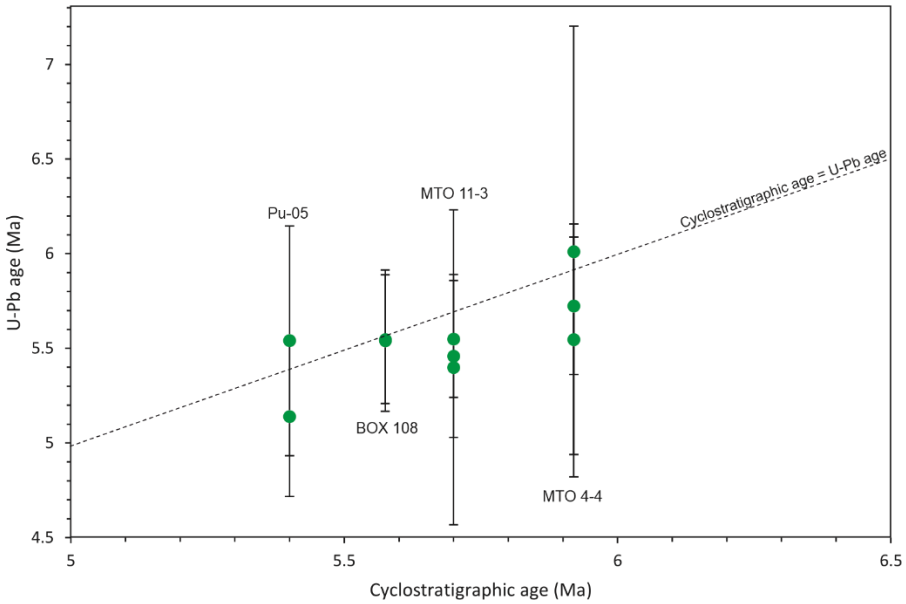

Fig. 5: Comparison of the obtained U-Pb ages and the expected cyclostratigraphic ages. The weighted mean of the offsets between both ages is -0.14 ± 0.14 Ma (±2σ). Dashed line represents the U-Pb age = cyclostratigraphic age correlation.

5.3 Pit depth profiles

Guillong et al. (2020) showed that different ablation parameters produce distinctive pit profiles (the so-called "aspect ratio" or depth/diameter ratio) and it could result in a noticeable bias in the data. The carbonate reference materials analysed here with a 130 µm spot size, resulted in a depth of ca. 15 µm (aspect ratio of 0.12), whereas the sulfates vary between 16 µm and 63 µm (aspect ratio between 0.12 and 0.48, Fig. 4). The ablation on NIST glass resulted in shallower ca. 10 µm deep holes and an aspect ratio of 0.13, similar to the carbonates. This divergence between the sulfates could be devoted to various non-excluding features such as different textures, particle size, porosity or compaction (Elisha et al., 2021). However, in the cases with an aspect ratio mismatch relative to the primary standard of less than 2, a deviation lower than 5% is anticipated (Guillong et al., 2020), which lies in the final result uncertainty of the majority of the samples analysed here. The larger discrepancy observed in the sample Pu 05 (relative mismatch of 4) could result in age offsets up to 10 % (Guillong et al., 2020, their Figure 4). However, Fig. 4b reveals an important heterogeneity in the pit profile in some samples, with a silhouette that resembles pores. Whether they correspond to porosity or chunks released due to a badly coupled laser beam, the signal remained stable. These pit depth issues are also related to the downhole fractionation corrections. Mangenot et al. (2018) claimed that shallow pit depth compared to the spot size could minimize the downhole fractionation. That argument could apply to our reference

materials and sulfates with shallower pit depth, but how it affects depths beyond 50-60 µm can be arguable. Lenoir et al., (2021) obtained coherent regression lines in fluorites even with pit depths (up to 50 % variable) larger than spot sizes. Notwithstanding, the lack of bias between our U-Pb ages and cyclostratigraphic ages suggests that the different downhole fractionation is not noticeable or remains within the uncertainties.

6 Conclusions

In this contribution, we have evaluated the applicability of carbonates as "almost-matrix-matched reference materials" for U-Pb dating of sulfates and for that purpose, gypsum and anhydrite samples from the Messinian Salinity Crisis were analysed. The known cyclostratigraphic ages of these evaporites were compared with the in-situ U-Pb ages obtained. The samples showed a high amount of common Pb and low spread in the U/Pb axis and therefore, only 15 % of the samples were successful. In fact, due to the large uncertainties obtained at the beginning, we were forced to switch from the SC-ICPMS to MC-ICPMS in order to improve the precision of the measurements. Four of the five successfully dated samples were indistinguishable within error from the expected ages, while the other was considerably younger. We assume that all the factors that could produce a bias in the final age, if any, are contained in the uncertainty and therefore, the use of carbonate reference materials could be a trustworthy approach for in situ U-Pb dating of sulfates. We acknowledge that the availability of sulfate reference material in the future will result in an improvement in both reliability and precision.

Author contributions

AB and AG were involved in the LA-ICPMS analysis and pit depth measurements. IV accomplished the fieldwork and sample collection. All the authors collaborated in preparing the manuscript.

Competing interest

The authors declare that they have no conflict of interest.

Acknowledgements

This study has benefited greatly from insightful reviews by Andrew R Kylander-Clark, Catherine Mottram and the associated editor Noah McLean, as well as the handling editor Klaus Mezger. This is FIERCE contribution No. 110. FIERCE is financially supported by the Wilhelm and Else Heraeus Foundation and by the Deutsche Forschungsgemeinschaft, which is gratefully acknowledged. Cores from Borehole EMS-4 (Cattolica Eraclea) in the Caltanissetta Basin (Sicily) are stored in the core repository of the University of Milano, Department of Earth Science "Ardito Desio" after core restoration performed within COST Action CA15103 MEDSALT.

365 **Table S1: U-Pb data of the LA-SC-ICP-MS measurements.**

Analysis number	name / sample	$^{207}Pb^a$ (cps)	U^b (ppm)	Pb^b (ppm)	$\frac{Th^b}{U}$	$\frac{^{238}U^c}{^{206}Pb}$	±2σ (%)	$\frac{^{207}Pb^c}{^{206}Pb}$	±2σ (%)
U436	MTO 4-4	11732	0.075	0.027	0.167	11.7	12	0.8208	3.2
U438		197284	0.26	0.46	0.324	2.04	15	0.8269	0.80
U447		1526928	0.96	3.9	0.182	0.85	11	0.8307	0.41
U448		28825	0.034	0.066	0.335	1.94	22	0.8350	1.6
U449		25729	0.52	0.058	0.140	34.4	8.4	0.8024	1.6
U450		10535	0.34	0.024	0.105	51.4	7.2	0.8019	1.8
U451		103061	0.97	0.23	0.374	15.9	11	0.8170	0.81
U453		84862	0.67	0.19	0.108	13.9	15	0.8182	0.71
U455		813450	1.1	1.9	0.133	2.28	12	0.8266	0.50
U456		434819	0.82	0.95	0.156	3.53	6.1	0.8333	0.51
U457		334973	0.16	0.82	0.162	0.70	21	0.8373	0.80
U458		137635	0.92	0.35	0.127	8.87	15	0.8230	0.77
U459		122106	0.41	0.25	0.138	7.28	9.8	0.8248	0.85
U460		66245	1.1	0.16	0.137	24.4	7.2	0.8096	1.2
U461		96692	1.7	0.24	0.129	23.0	7.8	0.8195	0.87
U463		153816	1.3	0.39	0.166	11.9	6.6	0.8224	0.84
U464		533967	1.5	0.96	0.148	10.0	13	0.8292	0.70
U465		198998	1.8	0.45	0.125	15.5	7.4	0.8195	0.70
U466		230504	0.82	0.58	0.225	5.05	7.3	0.8241	0.66
U467		16206	0.006	0.049	1.081	0.40	25	0.8295	2.1
U468		392950	1.6	0.87	0.102	7.47	9.5	0.8230	0.57
U469		142184	0.56	0.34	0.183	5.90	6.3	0.8285	0.75
U470		105200	1.2	0.25	0.107	17.7	6.2	0.8231	0.76
U471		165896	1.2	0.41	0.137	10.5	13	0.8235	0.82
U472		101404	0.73	0.26	0.361	9.16	12	0.8246	1.2
U473		139917	2.0	0.35	0.113	19.0	6.2	0.8173	0.66
U474		309796	1.7	0.74	0.117	8.42	9.4	0.8193	0.76
U475		190576	2.0	0.48	0.106	14.0	15	0.8172	0.76
U476		489694	1.8	1.2	0.118	5.07	8.3	0.8288	0.51
U477		627160	1.5	1.6	0.164	3.30	19	0.8290	0.53
U479		62648	0.55	0.15	0.221	13.2	7.0	0.8186	0.91
U480		186988	0.59	0.40	0.277	6.27	11	0.8272	0.57
U481		65836	0.25	0.17	0.383	4.83	9.9	0.8266	0.82
U482		211822	1.9	0.53	0.214	12.5	6.0	0.8187	0.70
U576	MTO 11-3	62812	1.2	0.16	0.312	26.8	7.2	0.8138	0.93
U577		71210	1.6	0.18	0.208	29.9	11	0.8051	1.1
U578		27053	1.3	0.063	0.147	82.3	5.5	0.7775	1.2
U579		66175	1.1	0.16	0.325	25.3	5.2	0.8123	0.92
U580		73038	1.3	0.18	0.329	24.4	4.9	0.8092	1.0
U581		116332	0.92	0.31	0.613	10.0	5.6	0.8209	0.71
U582		183789	1.5	0.48	0.222	10.6	7.8	0.8152	0.68
U583		282627	2.0	0.73	0.304	9.60	6.3	0.8217	0.53
U584		216408	3.0	0.51	0.147	23.0	10	0.8181	0.61
U585		53627	0.56	0.12	0.336	20.2	15	0.8144	1.3
U586		93652	0.35	0.25	1.565	4.61	7.8	0.8251	0.71
U587		192319	1.5	0.47	0.235	11.9	14	0.8215	0.74
U588		350075	2.7	0.69	0.225	21.2	16	0.8154	0.70
U589		87555	0.27	0.23	2.507	3.88	6.3	0.8313	0.85
U590		298582	1.7	0.67	0.205	11.2	18	0.8216	0.68
U591		263989	3.5	0.50	0.133	42.5	13	0.7960	0.59
U592		137796	1.2	0.36	0.529	11.0	6.5	0.8182	0.63

[a] Within run background-corrected mean ^{207}Pb signal in cps (counts per second).
[b] U and Pb concentrations and Th/U ratio were calculated relative to the primary reference material.
[c] Corrected for background, within-run Pb/U fractionation (in case of $^{206}Pb/^{238}U$) and subsequently normalised to the primary reference material (ID-TIMS value/measured value).

Table S2: U-Pb data of the LA-MC-ICP-MS measurements.

Analysis number	name / sample	$^{207}Pb^{a}$ (cps)	U^{b} (ppm)	Pb^{b} (ppm)	$\frac{Th^{b}}{U}$	$\frac{^{238}U^{c}}{^{206}Pb}$	±2s (%)	$\frac{^{207}Pb^{c}}{^{206}Pb}$	±2s (%)	sequence
009_U	BOX 108	47348	1.5	0.12	0.072	20.2	5.3	0.8166	0.71	1
010_U		44263	1.1	0.056	0.227	29.8	6.6	0.8160	0.89	1
011_U		8120	0.30	0.019	0.132	24.5	6.7	0.8187	1.4	1
012_U		159615	0.70	0.39	0.221	2.86	15	0.8321	0.56	1
013_U		52758	1.7	0.11	0.151	24.4	7.1	0.8109	0.68	1
015_U		45815	1.2	0.10	0.141	18.7	5.8	0.8205	0.69	1
016_U		210465	0.67	0.50	0.144	2.11	5.8	0.8319	0.50	1
017_U		153200	1.1	0.20	0.168	9.09	11	0.8307	0.56	1
020_U		8660	1.3	0.021	0.088	91.9	5.6	0.7616	1.6	1
020_Ui		54426	1.1	0.11	0.099	15.0	5.7	0.8207	0.68	1
021_U		40138	1.3	0.081	0.115	26.1	13	0.8202	0.75	1
022_U		13276	2.0	0.034	0.056	90.5	4.3	0.7733	1.2	1
024_U		15689	0.50	0.036	0.066	21.7	4.8	0.8219	1.4	1
025_U		24934	0.77	0.061	0.175	20.2	8.6	0.8253	0.90	1
026_U		217333	1.4	0.49	0.144	4.35	7.4	0.8290	0.47	1
027_U		45280	4.3	0.12	0.358	54.8	4.0	0.8014	0.75	1
028_U		106376	4.2	0.26	0.357	25.8	6.8	0.8208	0.63	1
029_U		46138	1.1	0.11	0.518	15.4	9.0	0.8247	0.85	1
030_U		143271	1.3	0.31	0.098	6.51	12	0.8286	0.50	1
031_U		104559	1.0	0.26	0.136	6.34	3.5	0.8281	0.56	1
032_U		66441	0.94	0.15	0.330	9.64	5.2	0.8307	0.78	1
033_U		40961	1.8	0.099	0.123	28.1	4.8	0.8213	0.76	1
034_U		14702	1.1	0.035	0.115	47.2	5.1	0.7992	1.6	1
035_U		28122	1.1	0.067	0.066	24.8	10	0.8136	0.87	1
036_U		42203	0.59	0.10	0.081	9.23	9.2	0.8277	0.71	1
037_U		164255	1.1	0.37	0.141	4.77	15	0.8291	0.53	1
038_U		260017	1.8	0.49	0.098	5.78	11	0.8302	0.47	1
039_U		27954	1.1	0.054	0.241	30.8	5.5	0.8191	0.83	1
040_U		59629	0.96	0.13	0.690	11.9	3.6	0.8280	0.65	1
041_U		20142	1.2	0.047	0.064	39.2	11	0.8030	1.1	1
042_U		172098	0.87	0.46	0.329	2.98	12	0.8315	0.51	1
043_U		26953	0.61	0.040	0.040	24.1	8.6	0.8164	0.98	1
044_U		25995	1.1	0.063	0.145	27.4	5.9	0.8133	1.1	1
045_U		30038	0.94	0.071	0.149	20.8	12	0.8210	1.0	1
046_U		416821	0.98	0.73	0.071	2.14	27	0.8309	0.46	1
047_U		27537	1.6	0.050	0.339	49.5	9.3	0.7956	1.1	1
048_U		34116	1.5	0.083	0.233	28.9	3.3	0.8144	0.76	1
049_U		9837	1.2	0.023	0.102	80.1	3.2	0.7825	1.2	1
050_U		17639	5.7	0.054	0.031	158	6.9	0.7188	1.3	1
059_U		60318	1.9	0.15	0.204	20.3	5.9	0.8131	0.82	1
060_U		14510	1.1	0.030	0.101	57.8	5.7	0.7979	1.1	1
061_U		99693	0.90	0.23	0.098	6.17	11	0.8280	0.64	1
062_U		106403	1.4	0.23	0.078	9.36	6.6	0.8275	0.54	1
063_U		33943	1.4	0.049	0.192	43.1	8.4	0.7970	1.1	1
067_U		9178	0.25	0.019	0.192	20.5	4.6	0.8202	1.4	1
068_U		60040	3.4	0.14	0.063	37.8	7.1	0.8103	0.71	1
069_U		42920	3.3	0.11	0.060	48.0	6.5	0.8031	0.78	1
070_U		71312	2.1	0.18	0.069	18.8	8.0	0.8194	0.73	1
071_U		16427	1.6	0.040	0.036	60.6	6.5	0.7900	1.4	1
009_U	BCR 9644	1031	0.061	0.001	0.012	74.5	7.0	0.8324	3.9	2
010_U		87	0.006	0.000	0.006	68.3	11	0.8105	13	2
011_U		87	0.014	0.000	<0.001	156	10	0.7736	14	2
014_U		110	0.020	0.000	0.008	243	9.5	0.7783	13	2
015_U		343	0.016	0.000	0.003	109	9.3	0.8263	8.4	2
017_U		337	0.036	0.000	<0.001	130	9.7	0.8259	7.1	2
018_U		125	0.025	0.000	<0.001	221	9.0	0.7825	11	2
019_U		275	0.019	0.000	<0.001	201	9.5	0.7862	10	2
021_U		109	0.025	0.000	0.008	218	8.9	0.7236	11	2
022_U		470	0.029	0.000	0.009	241	9.8	0.7104	8.7	2
023_U		108	0.019	0.000	0.008	207	9.9	0.7573	12	2
024_U		141	0.030	0.000	0.002	246	8.1	0.8004	11	2
025_U		720	0.045	0.001	<0.001	119	6.9	0.8306	5.4	2
026_U		347	0.038	0.001	0.046	117	8.2	0.7971	6.9	2

370 **Table S2: continue…**

027_U		1796	0.57	0.002	0.007	489	19	0.6571	4.2	2
028_U		2103	0.020	0.003	0.032	9.58	9.5	0.8217	2.9	2
029_U		2505	0.62	0.002	0.002	577	21	0.6308	5.7	2
031_U		285	0.030	0.000	0.010	109	6.5	0.7944	7.0	2
032_U		1114	0.19	0.001	0.006	248	6.6	0.7212	4.3	2
033_U		148	0.059	0.000	0.009	361	8.7	0.6898	11	2
034_U		180	0.017	0.000	0.014	106	9.4	0.7711	9.8	2
035_U		73633	0.30	0.025	0.001	19.2	36	0.8220	0.93	2
036_U		200	0.006	0.000	0.043	31.0	11	0.8088	8.4	2
037_U		925	0.10	0.002	0.001	73.9	21	0.8161	5.5	2
039_U		406	0.068	0.001	0.005	164	8.8	0.7734	6.3	2
350_U		9048	0.48	0.016	0.019	46.4	7.7	0.8196	1.5	2
359_U		50690	0.64	0.079	0.057	12.7	11	0.8247	0.66	2
360_U		5648	0.62	0.009	0.009	110	5.9	0.7752	1.9	2
361_U		1218	0.11	0.002	0.010	82	8.4	0.7972	4.1	2
365_U		49349	0.54	0.061	0.039	14.1	9.0	0.8213	0.72	2
366_U		4943	0.040	0.007	0.018	8.69	21	0.8239	2.5	2
368_U		1226	0.021	0.002	0.058	17.4	8.1	0.8227	3.5	2
369_U		65958	0.25	0.12	0.111	3.32	13	0.8291	0.62	2
374_U		305	0.032	0.001	<0.001	92.1	7.1	0.7948	7.8	2
375_U		2308	0.087	0.003	0.014	52.4	12	0.8094	4.9	2
376_U		27934	0.78	0.032	0.020	38.4	11	0.8195	0.89	2
377_U		17604	1.0	0.035	0.005	44.7	10	0.8127	1.0	2
378_U		58189	0.63	0.082	0.012	12.1	15	0.8195	0.62	2
382_U		9122	0.93	0.015	0.007	96.1	5.6	0.7875	1.5	2
384_U		882	0.019	0.001	0.099	21.3	18	0.8240	4.5	2
387_U		6049	0.32	0.008	0.010	61.4	13	0.8097	1.8	2
388_U		6781	0.52	0.010	0.008	79.6	11	0.8000	1.6	2
389_U		6780	1.2	0.010	0.002	183	11	0.7553	2.3	2
390_U		17237	0.90	0.028	0.015	50.3	6.2	0.8145	1.1	2
391_U		1518	0.11	0.002	0.008	74.1	10	0.8176	3.3	2
392_U		6719	0.40	0.008	0.008	82.2	4.7	0.7937	1.7	2
160_U	MTO 4-4	42459	0.071	0.033	0.124	3.46	16	0.8322	0.76	2
161_U		36404	0.100	0.024	0.086	6.60	10	0.8274	0.80	2
162_U		29300	0.31	0.025	0.119	19.6	15	0.8157	0.81	2
164_U		107586	0.65	0.064	0.107	16.1	12	0.8229	0.62	2
166_U		62776	1.1	0.055	0.129	32.1	4.3	0.8194	1.1	2
167_U		111666	0.47	0.12	0.163	6.31	15	0.8264	0.55	2
168_U		86330	0.82	0.076	0.115	17.1	7.0	0.8159	0.59	2
169_U		361703	0.88	0.24	0.100	5.74	15	0.8268	0.43	2
170_U		635386	0.50	0.56	0.142	1.43	11	0.8318	0.49	2
171_U		124867	0.27	0.083	0.109	5.25	16	0.8296	0.55	2
174_U		39215	0.67	0.032	0.075	33.2	9.4	0.8066	0.78	2
177_U		51601	0.29	0.049	0.109	9.37	8.3	0.8236	0.72	2
178_U		109476	1.3	0.079	0.093	26.2	11	0.8123	0.60	2
179_U		239957	0.80	0.19	0.117	6.47	9.5	0.8249	0.47	2
180_U		296212	0.93	0.23	0.126	6.50	15	0.8244	0.45	2
181_U		361123	0.98	0.35	0.082	4.50	13	0.8251	0.43	2
182_U		178465	0.91	0.12	0.142	12.4	5.1	0.8252	0.51	2
183_U		39048	0.49	0.037	0.067	21.4	8.1	0.8182	0.96	2
184_U		1048150	0.65	0.94	0.046	1.09	3.9	0.8279	0.39	2
185_U		102247	0.84	0.090	0.101	14.8	8.1	0.8206	0.61	2
186_U		121692	1.0	0.11	0.104	14.4	5.0	0.8202	0.50	2
187_U		198711	0.62	0.14	2.606	6.83	7.4	0.8273	0.47	2
188_U		291589	1.2	0.27	0.110	6.74	6.3	0.8238	0.43	2
189_U		231299	1.1	0.18	0.137	9.69	8.5	0.8269	0.45	2
190_U		413220	0.81	0.35	0.115	3.67	5.6	0.8296	0.42	2
191_U		11917	0.074	0.008	0.136	13.8	9.4	0.8215	1.4	2
192_U		126152	0.96	0.12	0.092	12.8	11	0.8217	0.62	2
193_U		73154	0.75	0.062	0.286	19.2	10	0.8187	0.86	2
194_U		549529	0.61	0.49	0.133	1.98	12	0.8351	0.45	2
197_U		51681	0.30	0.046	0.318	10.4	9.6	0.8230	0.72	2
198_U		273244	0.68	0.23	0.200	4.66	9.0	0.8330	0.45	2
209_U		477618	0.84	0.36	0.116	3.65	17	0.8277	0.41	2
210_U		412526	1.0	0.30	0.103	5.47	9.2	0.8287	0.43	2

Table S2: continue…

211_U		293172	1.0	0.18	0.126	8.84	11	0.8263	0.45	2
212_U		555903	1.1	0.38	0.088	4.67	16	0.8287	0.41	2
213_U		76097	0.92	0.047	0.084	31.2	8.0	0.8095	0.68	2
214_U		346163	1.1	0.31	0.233	5.90	6.1	0.8265	0.43	2
215_U		120901	0.90	0.10	0.108	14.0	14	0.8228	0.53	2
217_U		262806	1.3	0.35	0.127	5.92	8.3	0.8314	0.44	2
219_U		127957	1.0	0.10	0.133	16.17	13	0.8172	0.58	2
220_U		7919	0.11	0.004	0.160	42.6	11	0.8090	1.8	2
221_U		148260	1.6	0.13	0.243	19.2	5.8	0.8175	0.48	2
222_U		128181	1.3	0.094	0.089	21.0	13	0.8179	0.55	2
223_U		307635	1.5	0.26	0.143	9.25	4.3	0.8249	0.44	2
225_U		254729	1.6	0.23	0.110	11.2	8.6	0.8251	0.48	2
226_U		355548	1.3	0.24	0.114	8.58	9.1	0.8241	0.43	2
227_U		156455	1.1	0.14	0.098	12.9	7.5	0.8222	0.50	2
228_U		681461	0.67	0.64	0.095	1.65	10	0.8295	0.45	2
229_U		95834	1.0	0.084	0.100	19.4	7.7	0.8180	0.57	2
231_U		157487	1.3	0.14	0.081	13.9	12	0.8220	0.50	2
232_U		3039	0.066	0.003	0.158	34.0	7.1	0.8091	3.0	2
233_U		118467	2.0	0.10	0.060	30.5	7.1	0.8138	0.51	2
234_U		133809	1.6	0.11	0.121	23.2	8.0	0.8166	0.52	2
235_U		168534	1.8	0.15	0.103	19.5	6.0	0.8155	0.52	2
236_U		220800	1.8	0.19	0.180	14.7	11	0.8218	0.47	2
237_U		246643	1.3	0.21	0.084	9.59	7.9	0.8252	0.46	2
238_U		379877	0.62	0.29	0.089	3.43	32	0.8280	0.44	2
239_U		217983	0.78	0.19	0.108	6.43	14	0.8287	0.49	2
240_U		412692	0.73	0.38	0.066	3.05	12	0.8311	0.45	2
241_U		48316	0.51	0.040	0.149	20.1	7.7	0.8204	0.64	2
244_U	MTO 11-3	31010	0.020	0.020	2.177	1.60	14	0.8367	1.0	2
245_U		24767	0.047	0.030	0.533	2.52	22	0.8298	0.98	2
247_U		63055	0.28	0.079	0.384	5.66	7.2	0.8300	0.68	2
248_U		99922	0.26	0.13	0.530	3.04	5.8	0.8329	0.55	2
249_U		16054	0.064	0.024	0.595	4.31	7.1	0.8338	1.1	2
250_U		95971	0.20	0.094	0.466	3.36	5.4	0.8268	0.57	2
259_U		20407	0.83	0.026	0.110	50.5	12	0.7972	1.1	2
260_U		1786	0.011	0.003	0.737	6.09	8.0	0.8376	3.1	2
265_U		124037	0.14	0.10	0.947	2.20	8.5	0.8317	0.55	2
266_U		19405	0.088	0.021	0.470	6.70	14	0.8330	1.0	2
268_U		145975	1.7	0.21	0.208	12.4	7.1	0.8255	0.58	2
269_U		136367	0.12	0.19	1.641	1.02	5.3	0.8312	0.51	2
271_U		12070	0.034	0.018	1.147	2.98	14	0.8323	1.2	2
272_U		55571	0.22	0.075	0.452	4.56	5.9	0.8267	0.65	2
274_U		9126	0.059	0.012	0.554	7.69	11	0.8312	2.2	2
275_U		11007	0.054	0.017	1.229	5.12	6.3	0.8262	1.2	2
276_U		58251	0.092	0.080	0.545	1.84	16	0.8373	0.67	2
277_U		112321	0.29	0.13	1.165	3.41	8.0	0.8274	0.55	2
278_U		18070	0.048	0.028	0.754	2.70	7.3	0.8292	0.93	2
279_U		105781	0.37	0.15	0.693	3.77	6.9	0.8304	0.54	2
281_U		153346	4.0	0.22	0.081	28.5	7.9	0.8107	0.51	2
282_U		141144	3.6	0.20	0.069	27.9	8.6	0.8121	0.52	2
283_U		70729	0.71	0.11	0.147	9.89	4.2	0.8229	0.59	2
284_U		57878	0.28	0.065	0.318	6.81	14	0.8344	0.67	2
285_U		179536	0.73	0.19	0.343	6.08	4.7	0.8349	0.48	2
286_U		201969	1.3	0.32	0.313	6.39	4.9	0.8261	0.44	2
287_U		374142	2.5	0.56	0.055	7.10	7.0	0.8247	0.42	2
288_U		128171	3.2	0.18	0.087	28.7	5.0	0.8112	0.58	2
289_U		136966	4.1	0.18	0.082	35.2	5.3	0.8090	0.53	2
290_U		107867	4.9	0.16	0.060	48.2	7.7	0.8005	0.57	2
291_U		106011	1.9	0.17	0.431	17.9	18	0.8193	0.65	2
292_U		61587	4.5	0.11	0.075	63.7	15	0.7965	1.1	2
293_U		91650	3.8	0.14	0.043	42.7	5.7	0.8084	0.58	2
294_U		80760	3.8	0.12	0.075	47.9	5.8	0.8000	0.66	2
295_U		67617	4.3	0.11	0.043	62.8	5.6	0.7921	0.67	2
436_U	Pu 05	1336	0.008	0.001	0.018	17.1	12	0.7968	3.4	2
440_U		3541	0.013	0.002	0.047	9.40	12	0.7993	3.3	2
441_U		5779	0.013	0.001	0.089	18.4	9.4	0.7958	2.4	2

Table S2: continue…

442_U		819	0.010	0.000	0.002	36.2	12	0.7929	4.3	2
444_U		3503	0.002	0.001	0.058	5.61	15	0.7931	2.7	2
445_U		1398	0.006	0.001	0.043	12.3	8.4	0.7884	3.4	2
463_U		2058	0.019	0.001	0.043	19.9	10	0.7828	3.4	2
464_U		2093	0.019	0.001	0.059	23.3	7.5	0.7863	2.9	2
465_U		1188	0.007	0.001	0.120	16.6	13	0.7885	4.6	2
466_U		7720	0.049	0.005	0.043	14.6	4.8	0.7909	1.6	2
467_U		2652	0.032	0.002	0.032	26.4	15	0.7822	3.6	2
468_U		51097	0.31	0.030	0.045	15.9	4.4	0.7918	0.65	2
469_U		39483	0.30	0.024	0.134	19.2	4.7	0.7889	0.77	2
470_U		18990	0.23	0.011	0.031	33.6	6.1	0.7832	0.96	2
472_U		77384	0.56	0.046	0.022	18.8	5.0	0.7925	0.58	2
473_U		42753	1.2	0.029	0.014	62.5	7.5	0.7622	0.78	2
474_U		38267	0.51	0.026	0.017	29.8	12	0.7871	0.98	2
475_U		6462	0.25	0.004	0.010	92.2	9.6	0.7538	2.3	2
476_U		55482	0.93	0.039	0.092	36.7	9.8	0.7884	0.89	2
477_U		24674	0.11	0.016	0.047	11.2	4.7	0.7968	1.0	2
478_U		2847	0.075	0.002	0.007	74.4	12	0.7544	2.4	2
479_U		70165	0.52	0.045	0.079	17.8	6.7	0.7906	0.60	2
480_U		184870	0.88	0.12	0.069	11.9	3.8	0.7968	0.48	2
481_U		11662	0.62	0.008	0.009	115.9	7.6	0.7352	1.2	2
483_U		1829	0.014	0.001	0.030	15.8	11	0.7971	3.2	2
486_U		652	0.003	0.001	0.032	8.75	22	0.7941	5.5	2
487_U		97239	1.4	0.060	0.019	36.7	4.6	0.7742	0.57	2
488_U		12860	0.70	0.009	0.006	122	8.9	0.7343	1.4	2
489_U		22723	0.84	0.014	0.011	89.9	4.9	0.7468	0.93	2
490_U		39877	0.51	0.026	0.013	30.4	6.1	0.7844	0.81	2
491_U		30830	1.0	0.014	0.016	114	16	0.7368	0.91	2
492_U		19082	1.0	0.014	0.013	107	10	0.7335	1.1	2
009_U	MTO 11-3	90036	2.9	0.29	0.135	31.5	10	0.8054	0.65	3
010_U		60711	4.8	0.19	0.058	80.1	4.6	0.7784	0.73	3
011_U		321269	3.1	0.97	0.363	10.3	6.6	0.8207	0.40	3
012_U		18890	1.8	0.061	0.081	92.4	6.5	0.7715	1.1	3
013_U		104308	2.0	0.32	0.118	20.0	8.7	0.8134	0.49	3
014_U		49427	2.4	0.13	0.076	72.2	11	0.7788	0.99	3
015_U		140824	4.3	0.43	0.140	32.1	4.3	0.8054	0.50	3
017_U		107005	3.6	0.34	0.083	34.1	5.5	0.8103	0.54	3
018_U		63650	0.60	0.19	0.299	10.7	7.3	0.8207	0.60	3
024_U		112992	0.55	0.35	0.925	5.08	9.5	0.8279	0.48	3
025_U		148314	0.57	0.45	0.767	4.29	9.0	0.8277	0.44	3
028_U		148368	3.1	0.40	0.115	29.5	11	0.8088	0.60	3
031_U		54347	2.1	0.17	0.075	42.6	8.5	0.7968	0.76	3
033_U		158602	3.3	0.50	0.230	21.7	4.9	0.8142	0.45	3
034_U		47147	0.31	0.14	0.382	7.79	5.9	0.8239	0.66	3
035_U		161917	3.2	0.50	0.345	20.4	5.5	0.8167	0.42	3
037_U		245790	3.2	0.68	0.233	17.1	6.7	0.8149	0.47	3
038_U		152560	4.6	0.48	0.138	30.0	6.2	0.8048	0.54	3
040_U		45567	2.2	0.14	0.113	50.7	5.5	0.7961	0.68	3
041_U		43416	0.35	0.14	0.429	8.46	8.0	0.8208	0.94	3
042_U		41614	0.27	0.13	0.393	7.04	7.3	0.8276	0.77	3
043_U		51784	0.32	0.16	0.428	6.70	5.5	0.8184	0.67	3
044_U		185745	4.0	0.53	0.191	26.2	8.7	0.8085	0.46	3
045_U		197622	1.6	0.58	0.115	9.50	18	0.8224	0.45	3
046_U		163159	3.2	0.52	0.148	19.6	7.1	0.8129	0.52	3
047_U		137303	3.2	0.45	0.168	21.8	6.0	0.8140	0.54	3
048_U		74586	3.5	0.24	0.098	47.1	5.7	0.7992	0.63	3
049_U		142496	4.4	0.45	0.137	31.3	4.5	0.8067	0.43	3
050_U		148349	4.8	0.45	0.140	36.4	6.6	0.8066	0.51	3
059_U		102822	3.0	0.32	0.184	30.0	6.2	0.8036	0.51	3
061_U		125428	3.2	0.40	0.157	25.6	6.9	0.8108	0.47	3
062_U		37071	1.1	0.13	0.132	23.4	9.8	0.8098	0.76	3
063_U		48032	0.78	0.16	0.124	15.9	6.3	0.8180	0.71	3
064_U		69242	0.51	0.21	0.575	8.44	13	0.8203	0.63	3
065_U		165434	4.1	0.51	0.060	26.3	9.2	0.8096	0.53	3
066_U		134214	5.5	0.42	0.085	41.7	9.2	0.7982	0.55	3

Table S2: continue…

067_U		35032	3.5	0.12	0.051	91.7	4.7	0.7642	0.82	3
068_U		197102	2.8	0.65	0.166	13.2	5.2	0.8204	0.40	3
069_U		152700	2.9	0.46	0.121	21.3	17	0.8147	0.57	3
071_U		108748	0.34	0.35	1.351	3.08	9.5	0.8266	0.52	3
072_U		170691	0.85	0.55	0.592	4.95	11	0.8292	0.52	3
073_U		9935	1.7	0.032	0.068	155	7.0	0.7228	1.5	3
074_U		92588	5.5	0.30	0.059	58.1	9.9	0.7929	0.77	3
009_U	Pu 05	2167	0.030	0.002	0.005	64.4	17	0.7620	3.1	4
011_U		642	0.003	0.001	0.018	12.1	16	0.8304	6.2	4
013_U		2053	0.002	0.002	0.062	4.61	6.6	0.8177	2.8	4
014_U		550	0.011	0.000	0.005	75.7	18	0.7705	7.0	4
015_U		1351	0.027	0.001	0.001	67.1	8.5	0.7705	3.5	4
016_U		7081	0.10	0.006	0.015	56.5	7.6	0.7632	1.6	4
017_U		2027	0.064	0.002	0.009	133	9.8	0.7411	2.8	4
018_U		1355	0.051	0.001	0.004	127	15	0.7475	3.5	4
019_U		9372	0.10	0.007	0.018	63.1	8.6	0.7824	2.2	4
020_U		2028	0.015	0.002	0.013	27.0	6.9	0.7825	3.0	4
021_U		3008	0.011	0.002	0.004	18.5	5.1	0.8120	2.8	4
022_U		1140	0.005	0.001	0.010	13.2	19	0.7949	4.4	4
023_U		1051	0.033	0.001	0.003	94.7	16	0.7526	4.8	4
025_U		4316	0.059	0.004	0.007	52.0	14	0.7794	1.9	4
026_U		7481	0.050	0.007	0.022	23.4	9.4	0.7891	1.6	4
027_U		6387	0.028	0.006	0.010	12.9	18	0.7951	1.7	4
028_U		12431	0.023	0.011	0.002	6.39	14	0.8304	1.3	4
029_U		1118	0.023	0.001	0.007	73.5	9.6	0.7553	4.8	4
030_U		1099	0.004	0.001	0.000	6.04	35	0.8159	3.8	4
031_U		2456	0.003	0.002	0.029	4.92	11	0.8120	2.5	4
032_U		8610	0.057	0.007	0.042	29.4	9.7	0.7989	1.8	4
033_U		2450	0.006	0.002	0.086	8.36	7.5	0.8029	3.9	4
034_U		1943	0.010	0.001	0.029	22.9	6.7	0.8047	3.3	4
037_U		1471	0.010	0.001	0.014	23.4	12	0.8005	4.0	4
038_U		4241	0.057	0.003	0.008	79.3	9.5	0.7796	2.4	4
040_U		5569	0.039	0.005	0.049	25.9	6.2	0.8039	1.8	4
041_U		2789	0.008	0.002	0.015	10.5	20	0.8099	2.3	4
042_U		2272	0.022	0.002	0.007	35.6	20	0.8083	2.9	4
043_U		845	0.006	0.001	0.017	16.9	20	0.8020	4.5	4
044_U		1053	0.002	0.001	0.046	8.59	15	0.8135	3.7	4
045_U		2058	0.004	0.002	0.023	6.07	8.1	0.8143	2.8	4
046_U		1004	0.003	0.001	0.018	14.6	9.9	0.7973	3.8	4
047_U		1329	0.016	0.001	0.001	33.8	31	0.8012	3.7	4
048_U		1422	0.021	0.001	0.006	45.2	15	0.7810	3.1	4
049_U		276573	1.2	0.16	0.049	37.4	12	0.7884	0.56	4
060_U		1411	0.006	0.001	0.005	15.0	12	0.8117	3.0	4
061_U		7356	0.090	0.005	0.084	81.0	27	0.7538	2.1	4
062_U		1435	0.043	0.001	0.006	117	14	0.7277	3.2	4
064_U		633	0.056	0.001	0.001	219	23	0.6783	5.8	4
067_U		108576	0.66	0.094	0.019	21.2	4.2	0.8007	0.55	4
068_U		22860	0.23	0.019	0.017	37.3	4.5	0.7906	0.91	4
073_U		2091	0.14	0.002	0.002	199	9.7	0.6805	3.3	4
075_U		748	0.007	0.001	0.003	29.1	18	0.8043	4.8	4
078_U		1316	0.061	0.001	0.002	151	9.0	0.7338	3.7	4
079_U		2405	0.044	0.002	0.006	60.4	15	0.7854	2.5	4
080_U		2285	0.032	0.002	0.005	46.3	13	0.7933	2.8	4
081_U		2198	0.040	0.002	0.011	78.2	6.2	0.7541	2.5	4
088_U	MTO 4-4	154270	1.5	0.23	0.236	22.9	8.6	0.8128	0.51	4
089_U		66593	1.0	0.11	0.075	31.3	8.3	0.8050	0.64	4
092_U		25818	0.94	0.043	0.145	72.1	9.5	0.7867	1.3	4
093_U		188855	1.5	0.29	0.150	18.3	12	0.8136	0.45	4
094_U		70717	1.5	0.12	0.099	42.7	3.3	0.7971	0.68	4
095_U		392652	1.3	0.68	0.141	5.80	17	0.8244	0.40	4
096_U		39333	0.54	0.065	0.143	27.0	9.7	0.8107	0.72	4
098_U		343014	0.64	0.58	0.333	3.49	9.0	0.8302	0.43	4
099_U		15397	0.083	0.027	0.356	9.62	12	0.8195	1.2	4
100_U		35522	0.27	0.060	0.239	14.6	4.5	0.8160	0.78	4
109_U		202639	1.6	0.34	0.081	14.6	19	0.8141	0.57	4

Table S2: continue…

110_U		42283	0.70	0.069	0.083	33.9	5.6	0.8050	0.75	4
111_U		112583	1.5	0.19	0.099	25.5	9.2	0.8088	0.50	4
112_U		120520	0.70	0.21	0.043	10.4	16	0.8226	0.54	4
113_U		4129	0.17	0.007	0.067	75.4	9.7	0.7836	2.3	4
114_U		64831	0.23	0.12	0.051	6.23	6.3	0.8270	0.63	4
115_U		386587	2.3	0.63	0.061	11.8	8.6	0.8204	0.36	4
116_U		101833	0.059	0.18	0.585	1.01	20	0.8328	0.51	4
117_U		36664	0.023	0.066	0.931	1.06	21	0.8262	0.80	4
118_U		263914	1.5	0.45	0.110	10.7	10	0.8204	0.42	4
119_U		198490	1.0	0.33	0.157	10.3	10	0.8199	0.46	4
120_U		321214	1.3	0.54	0.099	7.66	5.1	0.8241	0.38	4
121_U		77903	0.53	0.13	0.046	12.6	6.3	0.8208	0.64	4
122_U		477392	1.1	0.81	0.133	4.04	11	0.8258	0.43	4
123_U		62459	0.84	0.11	0.089	25.6	12	0.8143	0.66	4
124_U		83446	0.45	0.14	0.130	9.87	14	0.8151	0.56	4
125_U		328913	0.86	0.53	0.114	5.22	11	0.8267	0.38	4
126_U		51257	1.2	0.080	0.082	53.2	6.5	0.7948	0.88	4
127_U		165366	1.2	0.28	0.094	13.1	6.3	0.8199	0.44	4
128_U		128085	0.78	0.24	0.136	9.83	15	0.8209	0.48	4
129_U		40122	0.48	0.068	0.076	22.5	8.6	0.8123	0.72	4
130_U		243432	1.6	0.40	0.112	12.9	8.9	0.8182	0.41	4
131_U		410018	1.0	0.63	0.098	5.57	9.6	0.8252	0.38	4
132_U		453513	1.3	0.75	0.108	5.30	13	0.8225	0.39	4
133_U		140762	1.0	0.23	0.102	14.5	10	0.8205	0.45	4
134_U		171451	1.8	0.25	0.114	27.1	5.9	0.8110	0.49	4
135_U		299485	1.3	0.50	0.088	8.65	7.3	0.8253	0.40	4
136_U		273271	0.95	0.46	0.126	6.74	7.5	0.8255	0.38	4
137_U		261422	1.00	0.44	0.167	7.25	8.8	0.8219	0.40	4
139_U		336303	1.2	0.56	0.199	6.73	14	0.8277	0.38	4
140_U		91664	0.34	0.15	0.108	7.23	15	0.8242	0.51	4
141_U		2833	0.13	0.005	0.158	98.4	7.1	0.7727	3.4	4
143_U		178759	0.87	0.30	0.089	9.14	10	0.8233	0.44	4
144_U		175078	1.1	0.30	0.101	11.7	18	0.8186	0.50	4
145_U		190119	1.2	0.30	0.112	13.5	8.7	0.8178	0.46	4
146_U		85820	1.4	0.15	0.221	30.2	3.5	0.8081	0.62	4
147_U		329223	0.75	0.55	0.140	4.28	9.5	0.8254	0.40	4
148_U		114269	1.1	0.20	0.094	18.2	8.5	0.8142	0.53	4
149_U		248241	1.1	0.42	0.103	8.31	8.3	0.8215	0.41	4
150_U		181792	0.92	0.28	0.100	11.7	10.0	0.8192	0.47	4
159_U		122725	0.83	0.21	0.168	12.6	5.4	0.8211	0.48	4
160_U		126548	0.90	0.22	0.102	12.7	8.3	0.8214	0.50	4
161_U		110684	1.9	0.17	0.086	39.1	4.6	0.8017	0.58	4
162_U		78280	1.2	0.13	0.092	30.3	7.1	0.8049	0.71	4
165_U		195480	1.0	0.34	0.092	9.69	9.0	0.8209	0.44	4
166_U		303135	1.3	0.49	0.115	8.74	7.7	0.8241	0.40	4
169_U		62163	0.87	0.11	0.079	22.9	9.7	0.8160	0.62	4
170_U		124538	1.1	0.21	0.093	17.9	7.9	0.8174	0.45	4
171_U		156199	1.3	0.27	0.089	15.8	13	0.8168	0.46	4
172_U		58090	0.92	0.094	0.090	33.5	7.6	0.8049	0.63	4
173_U		88433	1.5	0.14	0.102	40.5	7.9	0.7982	0.53	4
175_U		70717	1.1	0.11	0.100	35.0	6.1	0.8048	0.71	4
176_U		115260	1.2	0.15	0.099	39.4	5.0	0.8018	0.75	4
177_U		35514	0.82	0.058	0.079	47.4	5.3	0.7983	0.80	4
178_U		60006	1.5	0.090	0.095	59.1	8.5	0.7877	0.77	4
179_U		263568	1.7	0.45	0.091	11.8	9.8	0.8172	0.51	4
180_U		237512	1.2	0.38	0.089	10.4	26	0.8202	0.53	4
181_U		79587	1.0	0.14	0.118	24.4	5.7	0.8099	0.56	4
182_U		181676	1.5	0.31	0.156	15.2	8.6	0.8179	0.49	4
183_U		148496	0.62	0.39	0.155	3.83	6.4	0.8256	0.42	4
184_U		338583	1.7	0.59	0.067	9.12	8.8	0.8256	0.39	4
185_U		79508	1.1	0.13	0.065	26.5	4.1	0.8143	0.56	4
186_U		85236	0.73	0.15	0.089	15.8	9.9	0.8170	0.54	4
187_U		307851	1.0	0.53	0.256	5.90	13	0.8191	0.43	4
188_U		116771	1.1	0.21	0.087	16.2	11	0.8141	0.53	4
280_U	BOX 108	3723	0.027	0.015	0.018	4.21	34	0.8405	2.5	4

Table S2: continue…

283_U	215245	2.5	0.52	0.119	19.8	7.4	0.8240	0.47	4
284_U	95417	1.1	0.28	0.143	13.0	4.9	0.8259	0.51	4
287_U	9849	1.3	0.030	0.033	134	4.0	0.7471	1.5	4
288_U	11288	1.5	0.035	0.042	124	4.9	0.7493	1.6	4
289_U	34194	0.096	0.099	0.219	3.18	13	0.8344	0.81	4
290_U	242588	2.0	0.72	0.184	8.87	7.6	0.8307	0.42	4
291_U	142226	1.3	0.40	0.106	10.6	12	0.8321	0.45	4
292_U	205563	1.8	0.52	0.114	13.3	8.8	0.8231	0.44	4
293_U	174825	1.0	0.41	0.054	11.0	18	0.8305	0.45	4
294_U	155002	1.8	0.44	0.145	14.1	3.5	0.8248	0.46	4
296_U	135623	1.4	0.34	0.254	16.7	9.9	0.8252	0.47	4
297_U	431598	1.3	1.1	0.344	4.62	9.7	0.8293	0.37	4
298_U	73380	1.8	0.22	0.027	26.1	9.7	0.8186	0.58	4
299_U	285598	2.7	0.76	0.012	12.5	7.6	0.8291	0.43	4
300_U	177111	1.4	0.51	0.144	8.97	13	0.8245	0.46	4
309_U	20078	0.082	0.061	0.234	4.37	34	0.8415	1.4	4
311_U	162504	1.2	0.49	0.136	7.59	13	0.8274	0.50	4
312_U	300617	2.1	0.89	0.224	7.67	8.5	0.8305	0.42	4
313_U	4524	0.035	0.013	0.061	8.58	14	0.8286	2.2	4
314_U	149794	0.98	0.42	0.164	8.13	5.8	0.8278	0.46	4
315_U	151082	2.8	0.45	0.152	20.3	3.9	0.8208	0.45	4
316_U	403090	5.0	1.2	0.066	13.0	7.7	0.8299	0.41	4
317_U	66022	1.6	0.20	0.146	25.4	4.4	0.8132	0.62	4
318_U	69901	1.3	0.21	0.101	21.3	15	0.8190	0.62	4
319_U	43921	2.7	0.13	0.062	68.5	9.7	0.7921	0.79	4
320_U	95589	0.99	0.30	0.257	10.5	3.5	0.8274	0.49	4
321_U	86168	0.84	0.26	0.208	10.4	11	0.8324	0.54	4
322_U	45837	0.39	0.13	0.079	11.0	8.6	0.8248	0.70	4
323_U	81816	1.1	0.25	0.144	14.9	3.8	0.8234	0.61	4
324_U	291563	2.1	0.88	0.108	7.57	16	0.8275	0.44	4
325_U	54488	2.5	0.17	0.066	46.7	9.2	0.8017	0.66	4
326_U	166955	1.6	0.51	0.035	10.2	5.0	0.8268	0.48	4
327_U	378811	0.73	1.1	0.178	2.13	9.8	0.8380	0.40	4
328_U	125856	2.6	0.40	0.035	19.5	20	0.8257	0.64	4
330_U	157915	2.0	0.45	0.074	15.7	9.3	0.8244	0.48	4
331_U	245854	1.8	0.66	0.292	9.85	7.9	0.8210	0.58	4
332_U	47905	0.41	0.12	0.146	12.6	9.9	0.8276	0.76	4
333_U	566996	4.6	1.7	0.115	8.64	9.0	0.8295	0.38	4
334_U	84562	1.2	0.25	0.096	16.2	3.2	0.8216	0.55	4
335_U	66581	1.8	0.19	0.124	31.1	8.8	0.8126	0.64	4
336_U	192058	3.3	0.54	0.056	21.0	5.8	0.8238	0.44	4
337_U	82708	1.7	0.25	0.140	21.9	5.4	0.8239	0.50	4
338_U	99827	2.1	0.30	0.191	22.0	6.9	0.8194	0.51	4
339_U	49540	1.6	0.15	0.091	33.1	11	0.8110	0.65	4
340_U	209779	1.5	0.61	0.143	8.33	28	0.8299	0.49	4
341_U	93794	0.90	0.26	0.086	12.0	6.9	0.8256	0.51	4
342_U	44297	1.6	0.12	0.051	50.3	5.0	0.7976	0.81	4
343_U	16242	0.025	0.049	0.356	1.66	30	0.8431	1.3	4
344_U	74235	0.35	0.21	0.297	5.54	4.8	0.8306	0.54	4
345_U	195664	1.3	0.54	0.112	8.89	6.4	0.8261	0.44	4
346_U	48143	0.61	0.12	0.149	22.8	3.8	0.8228	0.73	4
348_U	71996	0.59	0.20	0.094	10.8	4.2	0.8295	0.57	4
349_U	102507	1.1	0.30	0.259	12.2	15	0.8253	0.50	4
350_U	198463	2.5	0.51	0.035	18.8	9.3	0.8261	0.44	4
359_U	8939	0.043	0.024	0.446	6.14	27	0.8324	1.6	4
360_U	57033	0.98	0.17	0.238	18.1	9.6	0.8228	0.61	4
361_U	203520	4.3	0.62	0.069	22.0	12	0.8204	0.40	4
362_U	35763	2.9	0.11	0.038	80.6	6.4	0.7848	0.83	4
364_U	79345	1.4	0.25	0.083	17.8	4.7	0.8228	0.53	4
365_U	39697	2.2	0.12	0.096	59.5	4.7	0.7974	0.71	4
366_U	144201	0.82	0.43	0.118	6.09	16	0.8321	0.46	4
367_U	53472	0.69	0.16	0.088	13.5	8.2	0.8254	0.67	4
369_U	50693	2.5	0.16	0.102	49.3	7.4	0.7975	0.74	4
370_U	52833	2.4	0.17	0.076	44.7	6.3	0.8078	0.59	4
371_U	51179	0.82	0.16	0.112	16.6	14	0.8172	0.80	4

Table S2: continue…

372_U		14847	0.28	0.040	0.050	25.5	12	0.8150	1.3	4
373_U		67995	0.55	0.20	0.083	8.70	13	0.8239	0.64	4
374_U		169346	1.3	0.47	0.106	9.98	12	0.8279	0.45	4
375_U		73258	1.4	0.23	0.113	19.1	10	0.8199	0.56	4
376_U		30039	0.42	0.097	0.077	13.1	14	0.8220	0.77	4
377_U		243980	1.9	0.75	0.154	8.1	4.6	0.8310	0.40	4
378_U		28838	1.6	0.089	0.085	58.1	5.3	0.7966	0.95	4
379_U		106946	2.6	0.33	0.039	24.9	5.1	0.8131	0.56	4
380_U		64981	2.6	0.19	0.102	44.2	5.7	0.8001	0.62	4
381_U		82318	2.1	0.21	0.091	39.3	13	0.8072	0.72	4
382_U		78516	1.3	0.24	0.098	17.0	12	0.8192	0.59	4
383_U	BCR 9644	22865	0.86	0.064	0.024	47.6	5.1	0.8056	0.97	4
384_U		6644	0.84	0.019	0.004	147	11	0.7724	2.0	4
386_U		77128	0.27	0.22	0.201	4.26	4.1	0.8256	0.55	4
388_U		3416	0.41	0.011	0.016	115	4.8	0.7689	2.2	4
390_U		18463	0.33	0.058	0.075	17.53	12	0.8061	1.0	4
392_U		4305	0.14	0.008	0.003	181	13	0.7574	3.8	4
393_U		14388	1.3	0.044	0.016	91.4	5.8	0.7816	1.2	4
394_U		18496	0.92	0.054	0.019	57.0	5.9	0.7943	1.1	4
395_U		4428	0.20	0.012	0.041	58.8	5.9	0.8002	2.0	4
396_U		12559	0.81	0.032	0.016	104	5.4	0.7788	1.5	4
397_U		1342	0.59	0.004	0.002	376	9.0	0.6875	4.7	4
399_U		146754	0.20	0.32	0.110	3.47	6.1	0.8260	0.55	4
409_U		11621	0.41	0.035	0.018	39.8	11	0.8117	1.5	4
411_U		5627	0.48	0.018	0.021	84.4	7.9	0.7917	1.8	4
412_U		23357	1.1	0.066	0.038	60.1	6.7	0.8029	0.97	4
413_U		14314	0.22	0.041	0.061	19.0	15	0.8151	1.2	4
415_U		6924	0.056	0.014	0.155	30.0	8.1	0.8014	4.3	4
416_U		6828	0.17	0.020	0.026	28.8	8.2	0.8266	1.7	4
423_U		4952	0.090	0.013	0.027	28.7	6.2	0.8009	2.2	4
427_U		962	0.047	0.003	0.102	42.2	11	0.8056	4.0	4
433_U		733	0.30	0.002	0.001	445	12	0.6898	6.1	4
435_U		3290	0.025	0.006	0.002	35.9	17	0.8262	4.6	4
438_U		1004	0.076	0.003	0.035	74.4	9.7	0.7965	4.1	4
440_U		891	0.007	0.003	0.025	8.70	10	0.8189	4.4	4
441_U		3306	0.47	0.010	0.002	139	5.6	0.7832	2.1	4
442_U		1782	0.18	0.005	0.002	104	4.6	0.7908	3.0	4
443_U		1876	0.10	0.005	0.002	68.3	5.5	0.8084	2.9	4
445_U		892	0.009	0.003	0.739	7.26	21	0.8357	4.3	4
446_U		5383	0.20	0.017	0.010	39.5	8.5	0.8110	1.6	4
447_U		5316	0.36	0.016	0.006	72.0	3.8	0.8105	1.7	4
448_U		4019	0.44	0.013	0.006	108	7.5	0.7851	3.3	4
449_U		839	0.16	0.002	0.005	236	9.6	0.7546	4.5	4
450_U		27342	1.5	0.084	0.040	56.2	8.4	0.8088	1.0	4
459_U		5280	0.17	0.017	0.016	31.9	19	0.8161	1.7	4
462_U		37636	0.062	0.11	0.226	1.78	9.2	0.8254	0.80	4
464_U		200339	2.3	0.61	0.050	11.8	6.9	0.8140	0.43	4
467_U		676	0.005	0.002	0.740	9.95	9.0	0.8126	5.2	4
468_U		1808	0.060	0.006	0.013	33.8	11	0.8128	3.0	4
469_U		3923	0.13	0.013	0.174	29.1	15	0.8056	2.1	4

[a] Within run background-corrected mean ^{207}Pb signal in cps (counts per second).
[b] U and Pb concentrations and Th/U ratio were calculated relative to the primary reference material.
[c] Corrected for background, within-run Pb/U fractionation (in case of $^{206}Pb/^{238}U$) and subsequently normalised to the primary reference material (ID-TIMS value/measured value).

References

Andreetto, F., Matsubara, K., Beets, C.J., Fortuin, A.R., Flecker, R., and Krijgsman, W.: High Mediterranean water-level during the Lago-Mare phase of the Messinian Salinity Crisis: insights from the Sr isotope records of Spanish marginal basins (SE Spain), Paleogeogr. Paleoclimatol. Paleoecol., 562, 110139, https://doi.org/10.1016/j.palaeo.2020.110139, 2021.

Astilleros, J.M., Godelitsas, A., Rodríguez-Blanco, J.D., Fernández-Díaz, L., Prieto, M., Lagoyannis, A., and Harissopulos, S.: Interaction of gypsum with Pb - bearing aqueous solutions, Appl. Geochem., 25, 1008-1016. https://doi.org/10.1016/j.apgeochem.2010.04.007, 2010.

Babel, M., and Schreiber, B.C.: Geochemistry of evaporites and evolution of seawater, in: Treatise on Geochemistry (2nd edition), edited by: Turekian, K., and Holland, H., Elsevier, Oxford, UK, 483-560, https://doi.org/10.1016/B978-0-08-095975-7.00718-X, 2014.

Brannon, J. C., Cole, S. C., Podosek, F. A., Ragan, V. M., Coveney, R. M., Wallace, M. W., and Bradley, A. J.: Th-Pb and U-Pb dating of ore-stage calcite and Paleozoic fluid flow, Science, 271, 491-493, https://doi.org/10.1126/science.271.5248.491, 1996.

Burisch, M., Walter, B. F. and Markl, G.: Silicification of Hydrothermal Gangue Minerals in Pb-Zn-Cu-Fluorite-Quartz-595 Baryte Veins, The Canadian Mineralogist, 55(3), 501-514, https://doi.org/10.3749/canmin.1700005, 2017.

Burisch, M., Gerdes, A., Meinert, L., Albert, R., Seifert, T., and Gutzmer, J.: The essence of time - fertile skarn formation in the Variscan Orogenic Belt, Earth Planet. Sci. Lett., 519, 165-170, https://doi.org/10.1016/j.epsl.2019.05.015, 2019.

CIESM: The Messinian salinity crisis from mega-deposits to microbiology, in: A consensus report. 33ème CIESM Workshop Monographs 33, edited by: Briand, F., CIESM Publisher, Monaco, 91-96, 2008.

Clauer, N., Chaudhuri, S., Toulkeridis, T., and Blanc, G.: Fluctuations of Caspian Sea level: beyond climatic variations? Geology, 28, 1015–1018, https://doi.org/10.1130/0091-7613(2000)28<1015:FOCSLB>2.0.CO;2, 2000.

Conley, R.F., and Bundy W.M.: Mechanism of gypsification, Geochim. Cosmochim. Acta, 15, 57-72, https://doi.org/10.1016/0016-7037(58)90010-3, 1958.

Costanzo, A., Cipriani, M., Feely, M., Cianfione, G., and Dominici, R.: Messinian twinned selenite from the Catanzaro Trough, Calabria, Southern Italy: field, petrographic and fluid inclusion perspectives, Carbonates and Evaporites, 34, 743–756. https://doi .org /10 .1007 /s13146 -019 -00516 -0, 2019.

Craig, G., Managh A.J., Stremtan, C., Lloyd, N.S., and Horstwood, M.S.A.: Doubling Sensitivity in Multicollector ICPMS Using High-Efficiency, Rapid Response Laser Ablation Technology, Anal. Chem., 90, 11564-11571, https://doi.org/10.1021/acs.analchem.8b02896, 2018.

Craig, G., Bracciali, L., and Lloyd, N.: LA-ICP-MS for U-(Th)-Pb geochronology: Which analytical capability is right for my laboratory? Thermo Fish. Sci. Smart. Note 30581, 2020.

Cruset, D., Verges, J., Rodrigues, N., Belenguer, J., Pascual-Cebrian, E., Almar, Y., Perez-Caceres, I., Macchiavelli, C., Trave, A., Beranoaguirre, A., Albert, R., Gerdes, A., and Messager, G.: U–Pb dating of carbonate veins constraining timing of beef

growth and oil generation within Vaca Muerta Formation and compression history in the Neuquen Basin along the Andean fold and thrust belt, Mar. Petrol. Geol., 132, 10520, https://doi.org/10.1016/j.marpetgeo.2021.105204, 2021.

Deng, X.D., Li, J.W., Luo, T., and Wang, H.Q.: Dating magmatic and hydrothermal processes using andradite-rich garnet U-Pb geochronometry, Contrib Mineral Petr., 172, 71, https://doi.org/10.1007/s00410-017-1389-2, 2017.

Elisha, B., Nuriel, P., Kylander-Clark, A., and Weinberger, R.: Towards in-situ U-Pb dating of dolomites, Geochronology 3, 337-349, https://doi.org/10.5194/gchron-3-337-2021, 2021.

Evans, N.P., Turchyn, A.V., Gázquez, F., Bontognali, R.R., Chapman, H.J., and Hodell, D.A.: Coupled measurements of $\delta^{18}O$ and δD of hydration water and salinity of fluid inclusions in gypsum from the Messinian Yesares Member, Sorbas Basin (SE Spain), Earth Planet. Sci. Lett., 430, 499–510, https://doi.org/10.1016/j.epsl.2015.07.071, 2015.

Flecker, R., and Ellam, R.M.: Identifying Late Miocene episodes of connection and isolation in the Mediterranean - Paratethyan realm using Sr isotopes, Sediment. Geol., 188-189, 189-203. https://doi.org/10.1016/j.sedgeo.2006.03.005, 1999

Flecker, R., Krijgsman, W., Capella, W., de Castro Martíns, C., Dmitrieva, E., Mayser, J.P., Marzocchi, A., Modestu, S., Lozano, D.O., Simon, D., Tulbure, M., van den Berg, B., van der Schee, M., de Lange, G., Ellam, R., Govers, R., Gutjahr, M., Hilgen, F., Kouwenhoven, T., Lofi, J., Meijer, P., Sierro, F.J., Bachiri, N., Barhoun, N., Alami, A.C., Chacon, B., Flores, Jose A., Gregory, J., Howard, J., Lunt, D., Ochoa, M., Pancost, R., Vincent, S., and Yousfi, M.Z.: Evolution of the Late Miocene Mediterranean Atlantic gateways and their impact on regional and global environmental change, Earth-Sci. Rev., 150, 365-392. https://doi.org/10.1016/j.earscirev.2015.08.007, 2015

Gerdes, A., and Zeh, A.: Combined U-Pb and Hf isotope LA-(MC-)ICP-MS analyses of detrital zircons: comparison with SHRIMP and new constraints for the provenance and age of an Armorican metasediment in Central Germany, Earth Planet. Sci. Lett., 249, 47-61, https://doi.org/10.1016/j.epsl.2006.06.039, 2006.

Gerdes, A., and Zeh, A.: Zircon formation versus zircon alteration — new insights from combined U-Pb and Lu-Hf in-situ LA-ICP-MS analyses, and consequences for the interpretation of Archean zircon from the Central Zone of the Limpopo Belt, Chem. Geol., 261 (3-4), 230-243, https://doi.org/10.1016/j.chemgeo.2008.03.005, 2009.

Grandia, F., Asmerom, Y., Getty, S., Cardellach, E., and Canals, A.: U-Pb dating of MVT ore-stage calcite: implications for fluid flow in a Mesozoic extensional basin from Iberian Peninsula, J. Geochem. Explor., 69, 377-380, https://doi.org/10.1016/S0375-6742(00)00030-3, 2000.

Grothe, A., Andreetto, F., Reichart, G.J., Wolthers, M., Van Baak, C.G., Vasiliev, I., Stoica, M., Sangiorgi, F., Middelburg, J.J., Davies, G.R., and Krijgsman, W.: Paratethys pacing of the Messinian Salinity Crisis: low salinity waters contributing to gypsum precipitation?, Earth Planet. Sci. Lett., 532, 116029, https://doi.org/10.1016/j.epsl.2019.116029, 2020.

Guillong, M., Wotzlaw, J.-F., Looser, N., and Laurent, O.: Evaluating the reliability of U-Pb laser ablation inductively coupled plasma mass spectrometry (LA-ICP-MS) carbonate geochronology: matrix issues and a potential calcite validation reference material, Geochronology, 2, 155-167, https://doi.org/10.5194/gchron-2-155-2020, 2020.

Horstwood, M. S. A., Košler, J., Gehrels, G., Jackson, S. E., McLean, N. M., Paton, C., Pearson, N. J., Sircombe, K., Sylvester, P., Vermeesch, P., and Bowring, J. F.: Community-derived standards for LA-ICP-MS U-(Th-) Pb geochronology-Uncertainty

propagation, age interpretation and data reporting, Geostand. Geoanal. Res., 40, 311-332, https://doi.org/10.1111/j.1751-908X.2016.00379.x, 2016.

Hsü, K.J., Ryan, W.B.F., and Cita, M.B.: Late Miocene desiccation of the Mediterranean, Nature, 242, 240-244, https://doi.org/10.1038/242240a0, 1973.

Hsü, K. J., Montadert, L., Ross, D.A., and Neprochnov, Y.P.: Annotated record of the detailed examination of Mn deposits from DSDP Leg 42 (Holes 372 and 379A). Pangaea, https://doi.org/10.1594/PANGAEA.871889, 1978. Supplement to: Worstell, P.J., Mélières, F., Bernoulli, D., Erickson, A.J., Wright, R., Bizon, G., Cita, M.B., Müller, C., Kidd, R.B., Fabricius, F.H., Garrison, R.E., Hsü, K.J., and Montadert, L.: Initial Reports of the Deep Sea Drilling Project. Initial Reports of the Deep Sea Drilling Project, U.S. Government Printing Office, XLII Pt. 1, 1249 pp + 1244 pp, https://doi.org/10.2973/dsdp.proc.42-1.1978, 1978.

Jochum, K. P., Weis, U., Stoll, B., Kuzmin, D., Yang, Q., Raczek, I., Jacob, D.E., Stracke, A., Birbaum, K., Frick, D.A., Günther, D., and Enzweiler, J.: Determination of reference values for NIST SRM 610–617 glasses following ISO guidelines, Geostand. Geoanal. Res., 35, 97–429, https://doi.org/10.1111/j.1751-908X.2011.00120.x, 2011.

Kameda, K., Hashimoto, Y., Wang., S.-L., Hirai, Y., and Miyahara, H.: Simultaneous and continuous stabilization of As and Pb in contaminated solution and soil by a ferrihydrite-gypsum sorbent, J. Hazard. Mater., 327, 171-179, https://doi.org/10.1016/j.jhazmat.2016.12.039, 2017.

Krijgsman, W., Hilgen, F. J., Raffi, I., Sierro, F. J., and Wilson, D. S.: Chronology, causes and progression of the Messinian Salinity Crisis, Nature, 400, 652-655, https://doi.org/10.1038/23231, 1999.

Krijgsman, W., Stoica, M., Vasiliev, I., and Popov, V. V.: Rise and fall of the Paratethys Sea during the Messinian Salinity Crisis, Earth Planet. Sci. Lett., 290 (1-2), 183-191, https://doi.org/10.1016/j.epsl.2009.12.020, 2010.

Krijgsman, W., Capella, W., Simon, D., Hilgen, F.J., Kouwenhoven, T.J., Meijer, P.T., Sierro, F.J., Tulbure, M.A., van den Berg, B.C.J., van der Schee, M., and Flecker, R.: The Gibraltar Corridor: watergate of the Messinian Salinity Crisis, Mar. Geol., 403, 238-246, https://doi.org/10.1016/j.margeo.2018.06.008, 2018.

Laskar, J.: The limits of Earth orbital calculations for geological time-scale use, in: Astronomical (Milankovitch) Calibration of the Geological Time-Scale, edited by: Shackleton, N.J., McCave, I.N., and Graham, P.W., Philos. Trans. R. Soc., Ser. A., 357(1757), 1735–1759. https://doi.org/10.1098/rsta.1999.0399, 1999.

Geochemistry of evaporites and evolution of seawater, in: Treatise on Geochemistry (2nd edition), edited by: Turekian, K., and Holland, H., Elsevier, Oxford, UK, 483-560, https://doi.org/10.1016/B978-0-08-095975-7.00718-X, 2014.

Lenoir, L., Blaise, T., Somogyi, A., Brigaud, B., Barbarand, J., Boukari, C., Nouet, J., and Pagel, M.: Uranium incorporation in fluorite and exploration of U-Pb dating, Geochronology, 3, 197-227, https://doi.org/10.5194/gchron-3-199-2021, 2021.

Lin, J., Sun, W., Desmarais, J., Chen, N., Feng, R., Zhang, P., Li, D., Lieu, A., Tse, J.S., and Pan, Y.: Uptake and speciation of uranium in synthetic gypsum ($CaSO_4 \cdot 2H_2O$): applications to radioactive mine tailings, J. Environ. Radioact., 181, 8-17, https://doi.org/10.1016/j.jenvrad.2017.10.010, 2018.

Liu, D.J., and Hendry, M.J.: Controls on ^{226}Ra during raffinate neutralization at the Key Lake uranium mill, Saskatchewan, Canada, App. Geochem., 26, 2113-2120, https://doi.org/10.1016/j.apgeochem.2011.07.009, 2011.

Ludwig, K.R.: User's Manual for Isoplot Version 3.75-4.15: a Geochronological Toolkit for Microsoft Excel, Berkeley Geochronological Center Special Publication, 5, 2012.

Lugli, S., Bassetti, M.A., Manzi, V., Barbieri, M., Longinelli, A., and Roveri, M.: The Messinian 'Vena del Gesso' evaporites revisited: characterization of isotopic composition and organic matter, J. Geol. Soc. Lond., 285, 179-190, http://dx.doi.org/10.1144/SP285.11, 2007.

Lugli, S., Manzi, V., Roveri, M., and Schreiber, B.C.: The primary Lower Gypsum in the Mediterranean: a new facies interpretation for the first stage of the Messinian salinity crisis, Palaeogeogr. Palaeoclimatol. Palaeoecol., 297, 83-99, https://doi.org/10.1016/j.palaeo.2010.07.017, 2010.

Mangenot, X., Gasparrini, M., Rouchon, V. and Bonifacie, M.: Basin-scale thermal and fluid flow histories revealed by carbonate clumped isotopes (Δ47) - Middle Jurassic carbonates of the Paris Basin depocentre, Sedimentology, 65(1), 123-150, https://doi.org/10.1111/sed.12427, 2018.

Manzi, V., Gennari, R., Lugli, S., Roveri, M., and Schreiber, B.C.: The Messinian "Calcare di Base" (Sicily, Italy) revisited, Geol. Soc. Am. Bull., 123, 347-370, https://doi.org/10.1130/B30262.1, 2011.

Manzi, V., Gennari, R., Hilgen, F., Krijgsman, W., Lugli, S., Roveri, M., and Sierro, F.J.: Age refinement of the Messinian salinity crisis onset in the Mediterranean, Terra Nova, 315-322, https://doi.org/10.1111/ter.12038, 2013.

Manzi, V., Gennari, R., Lugli, S., Persico, D., Reghizzi, M., Roveri, M., Schreiber, B.C., Calvo, R., Gavrieli, I., and Gvirtzman, Z.: The onset of the Messinian salinity crisis in the deep Eastern Mediterranean basin, Terra Nova 30 (3), 189-198, https://doi.org/10.1111/ter.12325, 2018.

Meilijson, A., Hilgen, F., Sepúlveda, J., Steinberg, J., Fairbank, V., Flecker, R., Waldmann, N.D., Spaulding, S.A., Bialik, O.M., and Boudinot, F.G.: Chronology with a pinch of salt: integrated stratigraphy of Messinian evaporites in the deep Eastern Mediterranean reveals long-lasting halite deposition during Atlantic connectivity, Earth-Sci. Rev. 194, 374-398. https://doi.org/10.1016/j.earscirev.2019.05.011, 2019

Millonig, L.J., Albert, R., Gerdes, A., Avigad, D., and Dietsch, C.: Exploring laser ablation U-Pb dating of regional metamorphic garnet - The Straits Schist, Connecticut, USA, Earth Planet. Sci. Lett., 552, 116589, https://doi.org/10.1016/j.epsl.2020.116589, 2020.

Montano, D., Gasparrini, M., Gerdes, A., Albert, R., Rohais, S., and Della Porta, G.: In-situ carbonate U-Pb analysis by LA-ICP-MS: From absolute dating to understanding the U-Pb partitioning in lacustrine systems, Goldschmidt 2019 Abstracts, 2323, 2019.

Montano, D., Gasparrini, M., Gerdes, A., Della Porta, G., and Albert, R.: In-situ U-Pb dating of Ries Crater lacustrine carbonates (Miocene, South-West Germany): implications for continental carbonate chronostratigraphy, Earth Planet. Sci. Lett., 568, 117011, https://doi.org/10.1016/j.epsl.2021.117011, 2021.

Montano, D., Gasparrini, M., Rohais, S., Albert, R., and Gerdes, A.: Depositional age models in lacustrine systems from zircon and carbonate U-Pb geochronology, Sedimentology, in press, https://doi.org/10.1111/sed.13000, 2022.

Morales, J., Astilleros, J.M., Jiménez, A., Göttlicher, J., Steininger, R., and Fernández-Díaz, L.: Uptake of dissolved lead by anhydrite surfaces, Appl. Geochem., 40, 89-96, https://doi.org/10.1016/j.apgeochem.2013.11.002, 2014.

Murray, R.C.: Origin and diagenesis of gypsum and anhydrite, J. Sedimen. Res., 34, 512-523, https://doi.org/10.1306/74D710D2-2B21-11D7-8648000102C1865D, 1964.

Natalicchio, M., Dela Pierre, F., Lugli, S., Lowenstein, T.K., Feiner, S.J., Ferrando, S., Manzi, V., Roveri, M., and Clari, P.: Did Late Miocene (Messinian) gypsum precipitate from evaporated marine brines? Insights from the Piedmont Basin (Italy), Geology, 42, 179–182, https://doi.org/10.1130/G34986.1, 2014.

Nuriel, P., Wotzlaw, J.F., Ovtcharova, M., Vaks, A., Stremtan, C., Šala, M., Roberts, N.M.W., and Kylander-Clark, A.R.C.: The use of ASH-15 flowstone as a matrix-matched reference material for laser-ablation U − Pb geochronology of calcite, Geochronology, 3, 35-47, https://doi.org/10.5194/gchron-3-35-2021, 2021.

Ossorio, M., Van Driessche, A.E.S., Pérez, P., and García-Ruiz, J.M.: The gypsum-anhydrite paradox revisited, Chem. Geol., 386, 16-21, https://doi.org/10.1016/j.chemgeo.2014.07.026, 2014.

Pagel, M., Bonifacie, M., Schneider, D. A., Gautheron, C., Brigaud, B., Calmels, D., Cros, A., Saint-Bezar, B., Landrein, P., Sutcliffe, C., and Davis, D.: Improving paleohydrological and diagenetic reconstructions in calcite veins and breccia of a sedimentary basin by combining Δ47 temperature, $\delta^{18}O$ water and U-Pb age, Chem. Geol., 481, 1-17, https://doi.org/10.1016/j.chemgeo.2017.12.026, 2018.

Parrish, R. R., Parrish, C. M., and Lasalle, S.: Vein calcite dating reveals Pyrenean orogen as cause of Paleogene deformation in southern England, J. Geol. Soc., 175, 425-442, https://doi.org/10.1144/jgs2017-107, 2018.

Petrash, D.A., Bialik, O.M., Bontognali, T.R.R., Vasconcelos, C., Roberts, J.A., McKenzie, J.A., and Konhauser, K.O.: Microbially catalyzed dolomite formation: From near-surface to burial, Earth-Sci. Rev., 171, 558-582, https://doi.org/10.1016/j.earscirev.2017.06.015, 2017.

Piccione, G., Rasbury, E.T., Elliott, B.A., Kyle, J.R., Jaret, S.J., Acerbo, A.S., Lanzirotti, A., Northrup, P., Wooton, K., and Parrish, R.R.: Vein fluorite U-Pb dating demonstrates post-6.2 Ma rare-earth element mobilization associated with Rio Grande rifting, Geosphere, 15, 6, 1958- 1972, https://doi.org/10.1130/GES02139.1, 2019.

Rasbury, E. T., and Cole, J. M.: Directly dating geologic events: U-Pb dating of carbonates, Reviews of Geophysics, 47(3), https://doi.org/10.1029/2007RG000246, 2009.

Rouchy, J.M., and Caruso, A.: The Messinian salinity crisis in the Mediterranean basin: a reassessment of the data and an integrated scenario, Sediment. Geol., 188–189, p. 35–67, https://doi.org/10.1016/j.sedgeo.2006.02.005, 2006.

Ring, U. and Gerdes, A.: Kinematics of the Alpenrhein-Bodensee graben system in the Central Alps: Oligocene/Miocene transtension due to formation of the Western Alps arc, Tectonics, 35, 1367-1391, https://doi.org/10.1002/2015TC004085, 2016.

Roberts, N. M. W., Rasbury, E. T., Parrish, R. R., Smith, C. J., Horstwood, M. S. A., and Condon, D. J.: A calcite reference material for LA-ICP-MS U-Pb geochronology, Geochem. Geophy. Geosy., 18, 2807-2814, https://doi.org/10.1002/2016GC006784, 2017.

Roberts, N. M. W., Drost, K., Horstwood, M. S. A., Condon, D. J., Chew, D., Drake, H., Milodowski, A. E., McLean, N. M., Smye, A. J., Walker, R. J., Haslam, R., Hodson, K., Imber, J., Beaudoin, N., and Lee, J. K.: Laser ablation inductively coupled plasma mass spectrometry (LA-ICP-MS) U-Pb carbonate geochronology: strategies, progress, and limitations, Geochronology, 2, 33-61, https://doi.org/10.5194/gchron-2-33-2020, 2020.

Roveri, M., Lugli, S., Manzi, V., and Schreiber, B.C.: The Messinian Sicilian stratigraphy revisited: toward a new scenario for the Messinian salinity crisis, Terra Nova, 20, 483-488, https://doi.org/10.1111/j.1365-3121.2008.00842.x, 2008a.

Roveri, M., Bertini, A., Cosentino, D., Di Stefano, A., Gennari, R., Gliozzi, E., Grossi, F., Iaccarino, S.M., Lugli, S., Manzi, V., and Taviani, M.: A high-resolution stratigraphic framework for the latest Messinian events in the Mediterranean area, Stratigraphy, 5, 323-342, 2008b.

Roveri, M., Flecker, R., Krijgsman, W., Lofi, J., Lugli, S., Manzi, V., Sierro, F.J., Bertini, A., Camerlenghi, A., De Lange, G., Govers, R., Hilgen, F.J., Hübscher, C., Meijer, P.T., and Stoica, M.: The Messinian Salinity Crisis: past and future of a great challenge for marine sciences, Mar. Geol., 352, 25-58, https://doi.org/10.1016/j.margeo.2014.02.002, 2014a.

Roveri, M., Lugli, S., Manzi, V., Gennari, R., and Schreiber, B.C.: High-resolution strontium isotope stratigraphy of the Messinian deep Mediterranean basins: implications for marginal to central basins correlation, Mar. Geol., 349, 113-125, https://doi.org/10.1016/j.margeo.2014.01.002, 2014b.

Ryan, W.B.: Decoding the Mediterranean salinity crisis, Sedimentology, 56 (1), 95-136, https://doi.org/10.1111/j.1365-3091.2008.01031.x, 2009

Schaltegger, U., Schmitt, A.K., and Horstwood, M.S.A.: U-Th-Pb zircon geochronology by ID-TIMS, SIMS, and laser ablation ICP-MS: Recipes, interpretations, and opportunities, Chem. Geol., 402, 89-110. https://doi.org/10.1016/j.chemgeo.2015.02.028, 2015.

Selli, R.: Il Messiniano Mayer-Eymar 1867. Proposta di un neostratotipo, Giornale di Geologia, 28, 1-33, 1960.

Seman, S., Stockli, D.F., and McLean, N.M.: U-Pb geochronology of grossular-andradite garnet, Chem. Geol., 460, 106-116, https://doi.org/10.1016/j.chemgeo.2017.04.020, 2017.

Sindern, S., Havenith, V., Gerdes, A., Meyer, F.M., Adelmann, D., and Hellmann, A.: Dating of anatase-forming diagenetic reactions in Rotliegend sandstones of the North German Basin, Int. J. Earth Sci., 108, 1275-1292, https://doi.org/10.1007/s00531-019-01705-x, 2019.

Sylvester, P.: Matrix effects in Laser ablation-ICP-MS, in: Laser Ablation-ICP-MS in the Earth Sciences: Current Practices and Outstanding Issues, edited by: Sylvester, P., Mineralogical association of Canada, 67-78, 2008.

Van Driessche, A.E.S., Stawski, T., and Kellermeier, M.: Calcium sulfate precipitation pathways in natural and engineering environments, Chem. Geol., 530, 119274. https://doi.org/10.1016/j.chemgeo.2019.119274, 2019.

Vasiliev, I., Mezger, E.M., Lugli, S., Reichart, G.J., Manzi, V., and Roveri, M.: How dry was the Mediterranean during the Messinian salinity crisis?, Paleogeogr. Paleoclimatol. Paleoecol., 471, 120-133, https://doi.org/10.1016/j.palaeo.2017.01.032, 2017.

Wafforn, S., Seman, S., Kyle, J.R., Stockli, D., Leys, C., Sonbait, D., and Cloos, M.: Andradite garnet U-Pb geochronology of the big Gossan skarn, Ertsberg-Grasberg mining district, Indonesia, Econ. Geol., 113, 769-778, https://doi.org/10.5382/econgeo.2018.4569, 2018.

Warren, J.K.: Evaporites: A Geological Compendium, Springer, Berlin, 1813 p, https://doi.org/10.1007/978-3-319-13512-0, 2016.

Warthmann, R., van Lith, Y., Vasconcelos, C., McKenzie, J.A., and Karpoff, A.M.: Bacterially induced dolomite precipitation in anoxic culture experiments, Geology, 28, 1091-1094, https://doi.org/10.1130/0091-7613(2000)28<1091:BIDPIA>2.0.CO;2, 2000.

Woodhead, J., Hellstrom, J., Maas, R., Drysdale, R., Zanchetta, G., Devine, P., and Taylor, E.: U-Pb geochronology of speleothems by MC-ICPMS, Quat. Geochronol., 1, 208-221, https://doi.org/10.1016/j.quageo.2006.08.002, 2006.

Woodhead, J., Hellstrom, J., Pickering, R., Drysdale, R., Paul, B., and Bajo, P.: U and Pb variability in older speleothems and strategies for their chronology, Quat. Geochronol., 14, 105-113, https://doi.org/10.1016/j.quageo.2012.02.028, 2012.

Yan, S., Zhou, R.J., Niu, H.C., Feng, Y.X., Nguyen, A.D., Zhao, Z.H., Yang, W.B., Qian, D., and Zhao, J.X.: LA-MC-ICP-MS U-Pb dating of low-U garnets reveals multiple episodes of skarn formation in the volcanic-hosted iron mineralization system, Awulale belt, Central Asia, GSA Bulletin, 132 (5-6), 1031-1045, https://doi.org/10.1130/B35214.1, 2020

Yang, Y.H., Wu, F.Y., Yang, J.H., Mitchell, R.H., Zhao, Z.F., Xie, L.W., Huang, C., Ma, Q., Yang, M., and Zhao, H.: U-Pb age determination of schorlomite garnet by laser ablation inductively coupled plasma mass spectrometry, J. Anal. At. Spectrom., 33, 231-239, https://doi.org/10.1039/c7ja00315c, 2018.

Zachariasse, W.J., van Hinsbergen. D.J.J., and Fortuin, A.R.: Mass wasting and uplift on Crete and Karpathos during the early Pliocene related to initiation of south Aegean left-lateral, strike-slip tectonics, Geol. Soc. Am. Bull., 120, 976–993, https://doi.org/10.1130/B26175.1, 2008.